2014

Reducing optical losses in organic photovoltaic devices using microlens arrays: theoretical and experimental investigation

Yuqing Chen
Iowa State University

Reducing optical losses in organic photovoltaic devices using microlens arrays: Theoretical and experimental investigation

by

Yuqing Chen

A dissertation submitted to the graduate faculty

in partial fulfillment of the requirements for the degree of

DOCTOR OF PHILOSOPHY

Major: Electrical Engineering

Program of Study Committee:
Sumit Chaudhary, Major Professor
Vikram L. Dalal
Rana Biswas
Santosh Pandey
Malika Jeffries-EI

Iowa State University

Ames, Iowa

2014

TABLE OF CONTENTS

LIST OF FIGURES

LIST OF TABLES

ACKNOWLEDGEMENTS

For me to finish this dissertation and my PhD program, I have to thank a number of people. First and foremost, I would like to thank my committee chair and major professor, Dr. Sumit Chaudhary. Thanks for his support and guidance. Without his help and patience on me, I can't image that I'm able to finish this whole PhD process. I also want to thank my committee members, Dr. Vikram Dalal, Dr. Rana Biswas, Dr. Santosh Pandey, and Dr. Malika Jeffries-EI, for their willingness to be on my committee, guidance and support throughout the course of this research. Thanks to Dr. Rana Biswas for the collaboration on the microlens project and providing simulation results with helpful discussions.

I want to offer my appreciation and thanks to friends and colleagues at Microelectronics Research Center (MRC) who have helped me with experiments, trainings and more. Thanks to Max Noack for his great help with equipment setup, maintenance, training and laughs. A special thanks to my labmates in Dr. Chaudhary's group: Rakesh Mahadevapuram, Moneim Ismail, John Carr, Kanwar Nalwa, Ryan Gebhardt, Tanvir Muntasir, and Aaron Thoeming. Thanks for the training, discussion, good conversations, collaboration, and hangouts. I'd like to thank other friends at MRC not only for working in the same building, but also for the good memories.

In addition, I would also like to thank my friends, colleagues, the department faculty and staff for making my time at Iowa State University a wonderful experience.

Finally, many thanks to my family for their encouragement and to my girlfriend for her hours of patience, respect and love.

ABSTRACT

Over the last decade, organic photovoltaic (OPV) devices have attracted a lot of attention and highest power conversion efficiencies (PCE) are now close to 10%. However, the performance is still much lower than that in the inorganic photovoltaic devices, like the widely commercialized silicon solar cells. There are many losses that can be contributed to the low efficiencies of OPV devices. Among them, optical loss is a big part, which can account for ~40% of total losses. The incident solar spectrum still largely remains poorly absorbed. In the OPV device structure, the thicknesses (~ 100-200 nm, at times less) are not enough to efficiently absorb light, and thicknesses cannot be indiscriminately increased further because of low charge carrier mobilities in most organic materials. Hence, to boost efficiencies further, it is imperative to improve light absorption within existing OPV architectures.

Here an optical structure - microlens array (MLA) - was employed to increase light absorption inside the active layer, and PCE of OPV devices increased even for optimized devices. Normal incident light rays are refracted at the MLA and travel longer optical paths inside the active layers. Three OPV systems - poly(3-hexylthiophene-2,5-diyl):(6,6)-phenyl C61 butyric acid methyl ester (P3HT:PCBM), poly[[9-(1-octylnonyl)-9H-carbazole-2,7-diyl]-2,5-thiophenediyl-2,1,3-benzothiadiazole-4,7-diyl-2,5-thiophenediyl]:(6,6)-phenyl C71 butyric acid methyl ester (PCDTBT:$PC_{71}BM$), and poly((4,8-bis[(2-ethylhexyl)oxy]benzo[1,2-b:4,5-b′]dithiophene-2,6-diyl)(3-fluoro-2-[(2-ethylhexyl)carbonyl] thieno[3,4-b]thiophenediyl)):(6,6)-phenyl C71-butyric acid methyl ester (PTB7:$PC_{71}BM$) were investigated. In the P3HT:PCBM system, MLA increased the absorption, absolute external quantum efficiency , and the PCE of an optimized device by ~ 4.3%. In the

PCDTBT:$PC_{71}BM$ system, MLA increased the absorption, absolute external quantum efficiency, and PCE by more than 10%. After optimizing the dimension of MLA, we observed up to 17% enhancement in the short circuit current of PCDTBT:$PC_{71}BM$ cells, and 10% enhancement in the short circuit current of PTB7:$PC_{71}BM$ cells. In addition, simulations incorporating optical parameters of all structural layers were performed and they support the enhancement of absorption in the active layer with the assistance of MLA. Theoretically and experimentally investigating several MLA dimensions, we found that photocurrent increases with the ratio of height to pitch size of MLA. Simulations reveal the enhancement mechanisms: MLA focuses light, and also increases the light path within the active-layer by diffraction. The results show that utilizing MLA is an effective strategy to further increase light absorption in OPV devices. Moreover, the MLA is on the substrate side opposite to the active layer and does not hinder the cell fabrication or electrical characteristics. It is also generally applicable to all types of solar cells due to its non-intrusive and external nature.

CHAPTER 1.
INTRODUCTION: ORGANIC PHOTOVOLTAIC DEVICES

1.1 Introduction to Photovoltaic Devices

In this era, fossil fuel based energy sources are depleting. The oil prices are rising and there are environment issues from using fossil fuel energy, which also contributes to the climate change. All these lead to more focus on renewable energy sources. The renewable energy is becoming more important also due to the political momentum towards its adoption. Among the renewable energy sources, direct conversation of solar energy to electricity using photovoltaic effect is very attractive due to the abundance of solar energy resource, which dwarfs all other energy resources combined. Solar electricity generation is now the fastest growing electricity source. In all, the world's installed photovoltaic (PV) generating capacity is now close to 140,000 megawatts--enough to power each home in Germany.[26]

1.1.1 History of Photovoltaic Devices

The story of PV devices can be dated back to 1839, when Becquerel discovered the photovoltaic effect after immersing a silver-coated platinum electrode into an electrolyte irradiated with light.[27] Since then there had been development of some early thin film cells in the 1930s, based on the Schottky barrier device. In 1953, Chapin came up with the concept of using thin films. The first thin film cell based on CdS was deposited on plastic in the early 1967. Soon after that some photovoltaic materials were discovered, including GaAs, InAs and CdTe. The simulation of cells based on these materials showed promising high efficiency. The design of multiple bandgap and tandem cells was also developed at that time. In the 1970s, thin films of crystalline silicon and a series of new semiconductor materials

were developed by scientists taking part in the US PV Research and Development Program. Almost all of the materials used today by PV industry were prototyped then. In the early 1980s, polycrystalline silicon thin film cell was developed by Barnett. Then Martin Green came up with a new design of burying wire contacts in thin grooves to increase surface area for incident light, leading to cells with efficiency of 20%. In 1997, Sharp commercialized the triple junction amorphous silicon cell. In 2007, Sanyo had a new design of solar cell called HIT (heterojunction with intrinsic thin layer) and obtained 22% efficiency cells. This HIT solar cell includes a single thin crystalline silicon layer surrounded by ultra-thin amorphous silicon layers. This HIT structure can reduce recombination loss and improve the overall output. GaAs cells have gone through rapid development and are efficient to power spacecraft now. The third generation solar cells are becoming more popular and increased in the production.

1.2 Organic Photovoltaic (OPV) Devices

Within the solar cell community, OPV devices have received heightened attention due to advantages such as flexibility, potentially low cost production, lightweight and easy integrability into building products, clothes and fabrics.

1.2.1 History of OPV Devices

The history of OPV devices can be dated back to 1954, when fairly good electrical conductivity was found in halogen doped organic compounds.[28] Even though many of them are not stable and can't keep the property for a long time, it's a working basis for the later development of OPV. With this interesting discovery, the studies of charge transport of small molecules had been done systematically in the following years.[29] Another breakthrough

discovery came in the late 1970s, when three main researchers got conductivity of polymer polyacetylene by doping with halogens and made their ways to Nobel Price in Chemistry in 2000.[30] The conductivity of carbon-based semiconductors is because of the alternation of single and double bonds between carbon atoms (a.k.a conjugation).[31] Since the discovery of conductivity in conjugated polymers and theirs applications in OPV devices, OPV devices have been making rapid progress in research and development in academia and industry; maximum power conversion efficiencies have increased from around 2% to 11% in the last decade.[32, 33] This progress is owing to the development of new materials, and novel device structures and processing conditions. So far, majority of studies on OPV devices have focused on the development of new materials[34-36], interlayers[7, 37, 38], and morphology optimization[39-43]. Another important way to enhance the PCE of OPV devices is by increasing light absorption inside the active layers using various optical approaches, which will be introduced and discussed more in the chapter 2.

1.2.2 Working Mechanism and Structures of OPV Devices

The device structure and working mechanism of conventional OPV is shown in **Fig. 1**. In an organic single-junction solar cell, illustrated in **Fig. 1**, the conversion of a photon into an electron–hole pair is able to do the work of qV_{oc} (q: electron charge and V_{oc}: open circuit voltage). This process typically takes six steps as follows, where η is the efficiency of each step:

1) Photon absorption (η_A): Photons with energy hv higher than the bandgap of donor (usually conjugated polymer) are absorbed. However, photons with energy a little less than the bandgap of donor might also be absorbed via subgap.[44] Because of the high absorption coefficient (ca. 10^5 cm^{-1}), conjugated polymers absorb light very efficiently at the maximum

of their absorption spectrum. As a result a layer thickness of only a few hundred nanometer is required to absorb all the light at their peak wavelength absorption. As a comparison to silicon based solar cells, active layer thicknesses of hundreds of micrometers are required since silicon is an indirect semiconductor.[45]

2) Exciton generation (η_{ex}): The absorbed photon energy excites electron-hole pair with opposite spins. The electron and hole are bound by coulomb attraction in a singlet exciton state, which has a binding energy around 0.3~0.5ev, much larger than inorganic excitons.[45]

3) Exciton diffusion (η_{diff}): The exciton diffusion length L_D, which characterizes the effective width of the active area of the polymer film at the acceptor interface, has been reported to be 5–8 nm in PPV based conjugated polymers. The exciton diffusion lengths in various conjugated polymers reported in the literature show a large variation, ranging from 5 to 20 nm.[45]

4) Exciton dissociation (η_{ed}): Organic semiconductors are characterized by low relative dielectric constants, typically ranging from 2 to 4. As a result, for a photogenerated electron and hole at the donor/acceptor interface the Coulomb binding energy can be very strong. As a result, the bound electron–hole pair either recombines or dissociates into free charge carriers when the carriers are able to escape their mutual Coulomb attraction. In molecular solids it is generally accepted that the photogeneration of charge carriers results from field- and temperature-assisted dissociation of singlet excitons.[45]

5) Charge transport (η_{tr}): After photoinduced excitons transfer at the donor/acceptor interface and subsequent dissociation, the electrons are localized in the PCBM phase whereas the holes remain in the polymer chains. Subsequently, the free electrons and holes must be transported

via percolated fullerene and polymer pathways towards the electrodes to produce the photocurrent.

6) Charge collection (η_{cc}): The free charge carriers are transported to the corresponding electrodes and collected by anode and cathode at the interface of electrode and organic semiconductor.

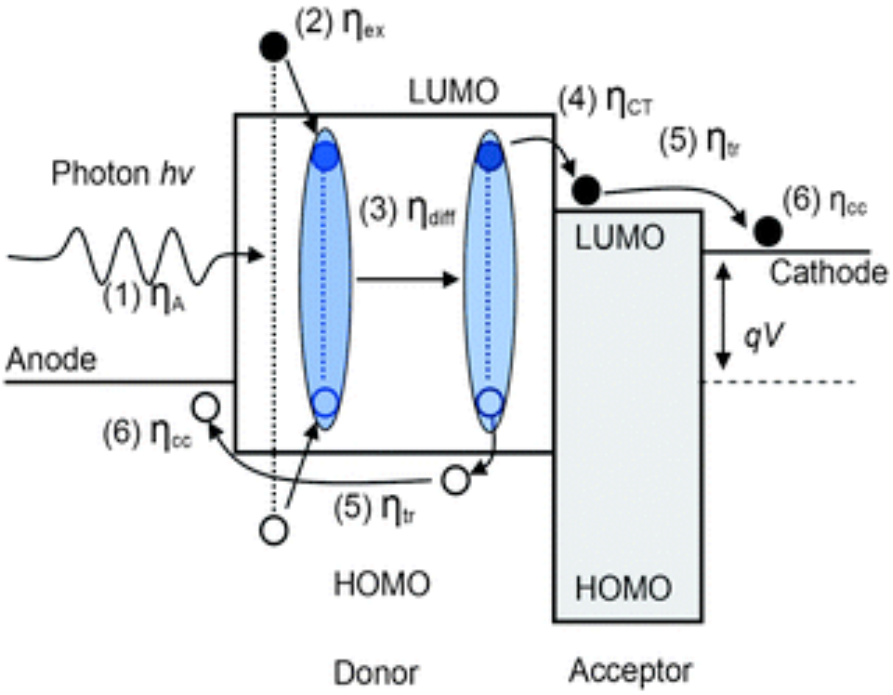

Fig.1 Energy level diagram of a donor–acceptor (D–A) polymer photovoltaic cell showing six steps associated in device operation. LUMO: lowest unoccupied molecular orbitals; HOMO: highest occupied molecular orbitals; and hv: photon energy.[24]

Associated with these steps in a single junction solar cell are limitations and losses that include:

(i) Absorption loss—Spectral mismatch leading to incomplete absorption of low energy photons;

(ii) Thermalization loss—Conversion of photon energy into a lower energy;

(iii) Exciton loss;

(iv) Energy loss required for exciton dissociation;

(v) Charge recombination.[24]

In order to improve device efficiency, the structure of OPV devices has gone through development. There have been four types of design of active layer structure in OPV, as illustrated in **Fig. 2**.[3] These four types are listed below and discussed:

1. Single layer: There's only one polymer, forming the active layer. It would suffer from exciton loss due to small exciton diffusion length (4~20nm).

2. Bilayer: Conjugated polymer and fullerene form the active layer with layer on another layer. Only photons absorbed within one exciton diffusion length to interface would have exciton dissociated.

3. Bulk heterojunction: Donor (conjugated polymer) and acceptor (fullerene) are mixed together to create interpenetrated layer. It has smaller domain so that there's more chance for excitons dissociation. This is the most studied structure, which gives the highest efficiency.

4. Ordered nanostructure: ideal structure; however suffering from back recombination and lower carrier mobility, not very successful yet.

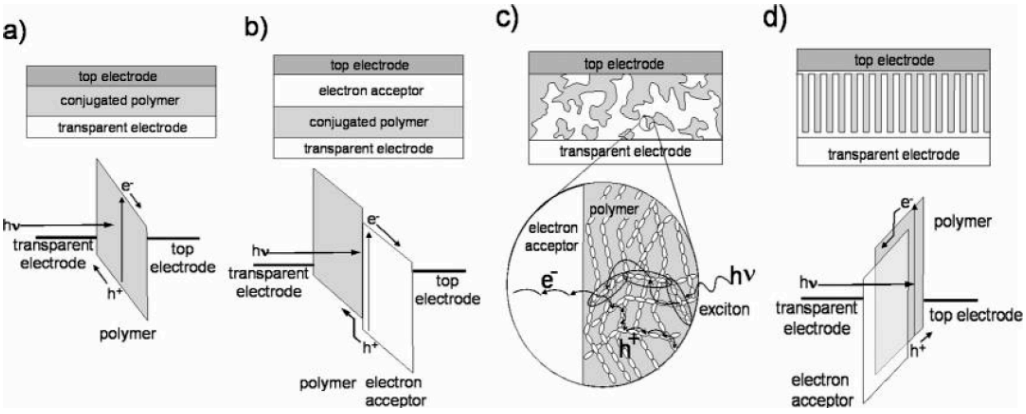

Fig. 2 Four device architectures of conjugated polymer-based photovoltaic cells: (a) single-layer PV cell; (b) bilayer PV cell; (c) disordered bulk heterojunction; (d) ordered bulk heterojunction.[3]

In the OPV devices, there are interlayers between active layer and electrodes. The introduction of proper interfacial materials to optimize the electronic and electrical properties between the interfaces of the light-harvesting active layer and the charge-collecting electrode has become an important criterion to improve the performance of polymer solar cells.[7] The interlayers are introduced to tune the energy level alignment at active layer/electrode interface. They also define the polarity of electrodes and improve charge selectivity as show

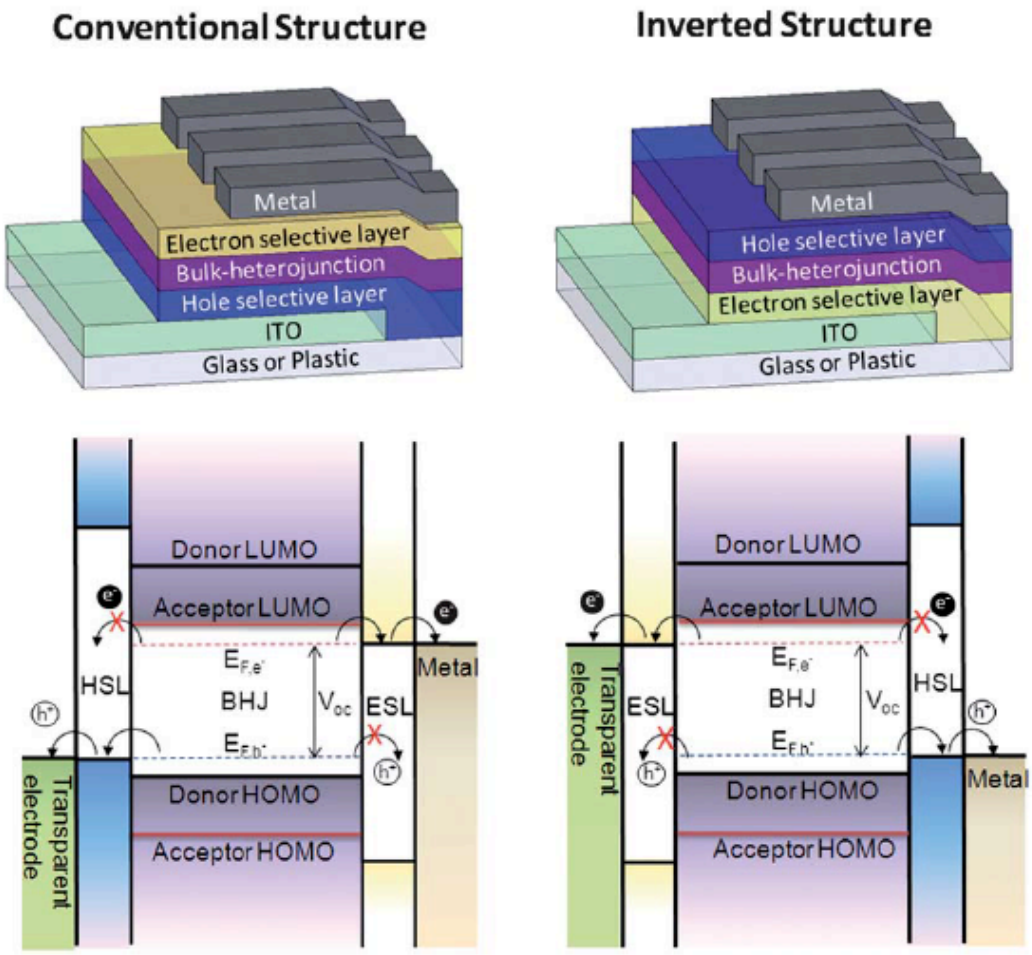

Fig. 3 Device architecture of conventional OPV (upper left) and inverted OPV (upper right). Schematic view of the energy level alignment in a conventional OPV (bottom left) and an inverted OPV (bottom right) with interfacial layers providing Ohmic contacts and charge selectivity at both electrodes.[7]

in **Fig. 3**. The interlayers can alter the morphology of active layer by controlling surface properties. The insertion of interlayers acts as optical spacers and provides plasmonic effect to module light absorption in the active layer. The interfacial stability between the active layer and electrodes can be improved.[7]

There are a lot of studies in the polymer materials of OPV devices. The development

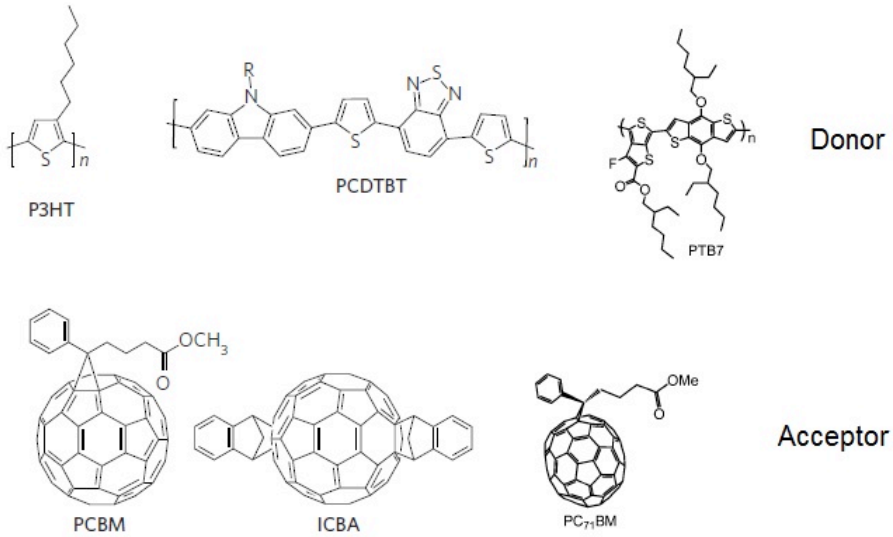

Fig. 4 Most studied material (donor and acceptor) employed in OPV devices

of these material systems helps improve the device efficiency and stability. The most studied materials employed in OPV devices are summarized in **Fig. 4**.

The development and improvement of OPV devices have also seen in nano-morphology optimization. The methods like solvent annealing can enhance OPV performance as seen in **Fig. 5** and **Fig. 6**.

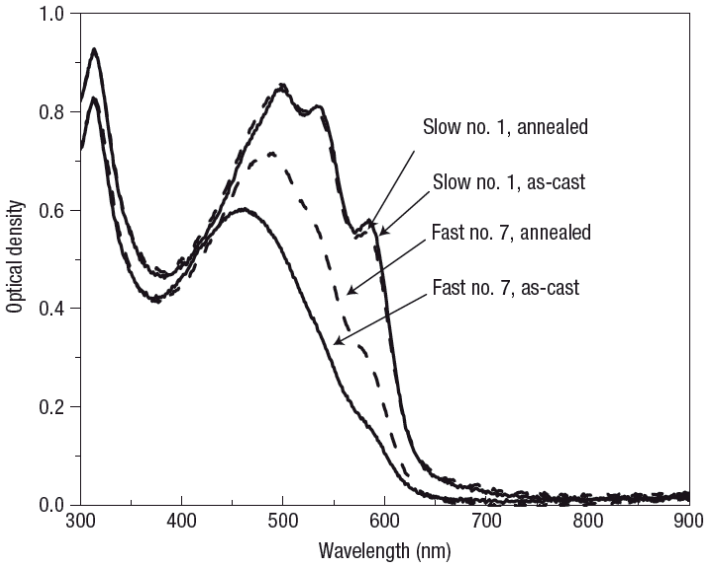

Fig. 5 Effect of film growth rate and thermal annealing on the absorbance of the P3HT/PCBM films. Ultraviolet–visible absorption spectra for films of P3HT/PCBM (in 1:1 wt/wt ratio), for both slow-grown (no. 1) and fast-grown (no. 7) films, before (solid line) and after (dashed line) annealing. The films were spun cast at 600 r.p.m. for 60 s (film thickness~210 nm) and the annealing was done at 110 ˚C for 20 min. [25]

Thermal annealing as another method to improve nano-morphology is also widely used and helps improve device performance. Thermal annealing is well known for strengthening, crystallization, and lattice repair of metal, inorganic and organic semiconductor. It improves OPV devices in polymer crystallization, hole mobility, J_{sc}, EQE, and efficiency as seen in **Fig. 7** and **Fig. 8**.

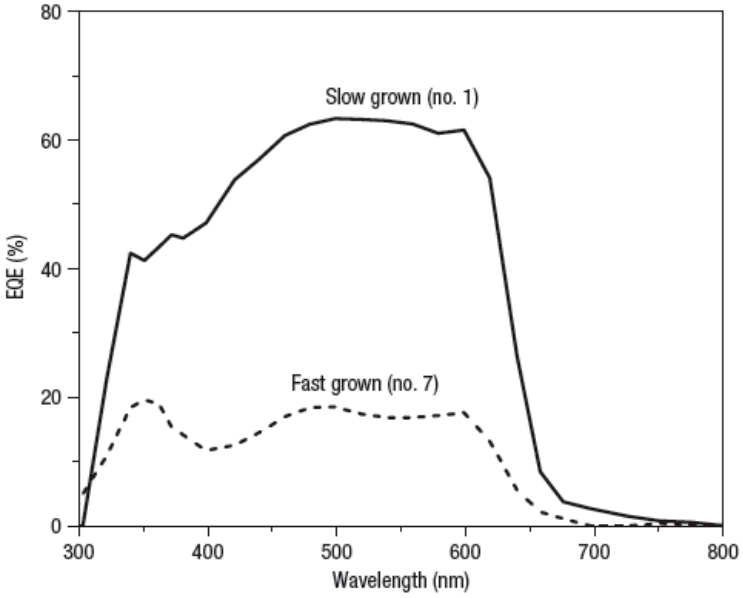

Fig. 6 Effect of film growth rate on EQE of polymer solar cells. EQE measurements are plotted for P3HT/PCBM photovoltaic cells for two types of active layer: slow grown (no. 1) and fast grown (no. 7). The efficiency maximum for slow-grown film is ~63% which is more than three times that of fast-grown film (~19%).[25]

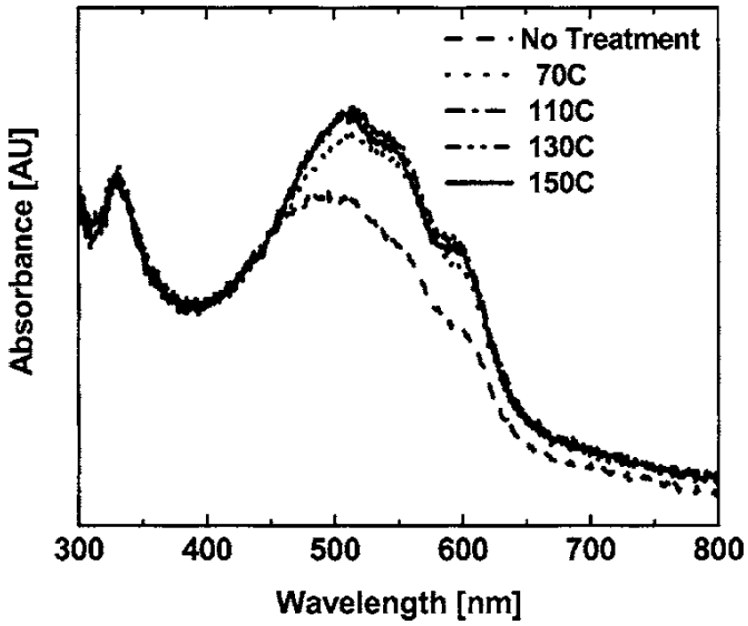

Fig. 7 UV-Vis absorption spectra obtained for P3HT:PCBM thin films with PCBM concentration=50 wt% before and after annealing at different temperatures. The annealing time here is 10 min for all the films.[23]

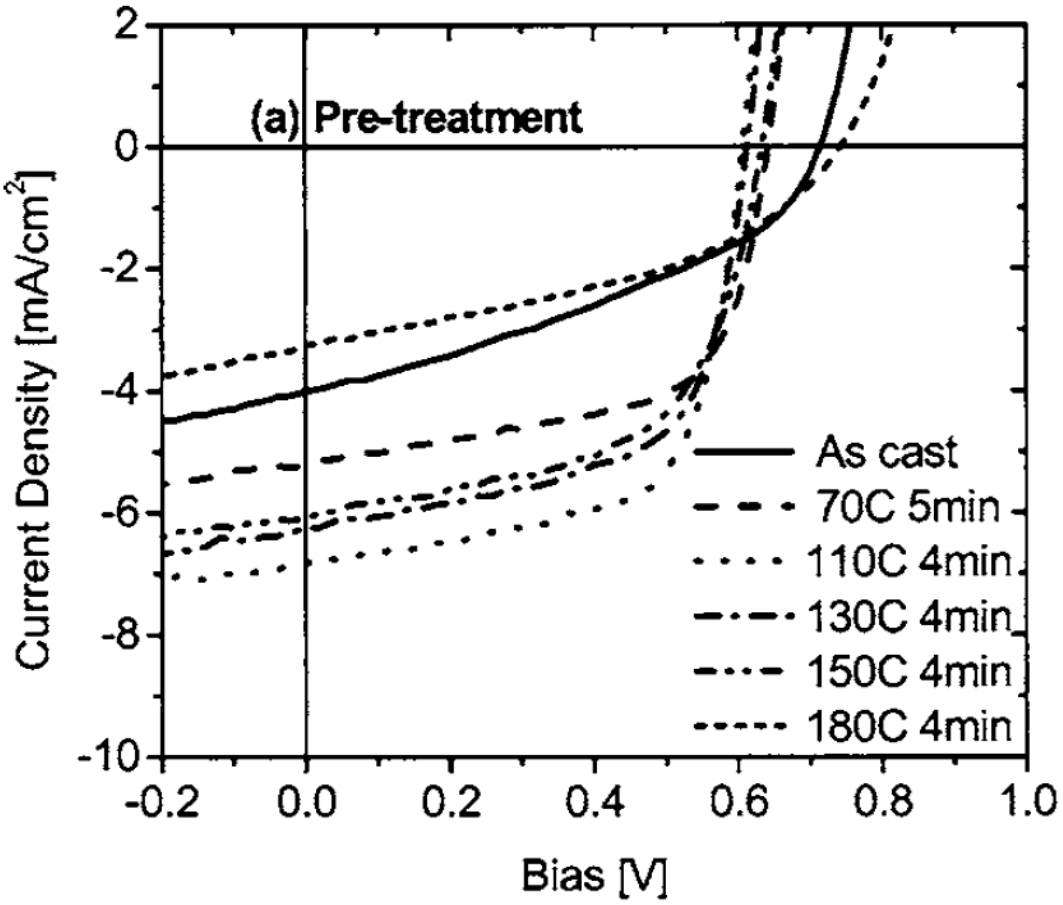

Fig. 8 I-V characteristics under an illumination of 100 mW/cm^2 AM1.5G for devices that have undergone annealing pretreatment treatment. The different curves represent different annealing temperatures ranging from RT to 180 °C.[23]

CHAPTER 2.

INTRODUCTION: PHOTON MANAGEMENT IN OPV DEVICES

2.1 Importance of Photon Management in OPV Devices

In order to absorb more light, it would be desired to have thicker photo absorbing layer (a.k.a. active layer) in solar cells. However, the thickness of active layer should not be too large. The device performance increases with active layer thickness at small thickness, but decreases after some optimum thickness. The optimum thickness is not designed to be very large to absorb all the light, instead a trade off between light absorption and electric properties. With the thickness increasing, more light would be absorbed definitely. The number of photons absorbed as a function of active layer thickness increases monotonically, but can not be described with a simple function due to interference effect.[46, 47] The visual relation between total photon absorption and active layer thickness can be referred in Figure 5b of [Dibb 2013]. Figure 6 of [Dibb 2013] even clearly shows the distribution of photon absorption with active layer thickness through contour plots of absorption in the active layer. However, the converting percentage of photons to collected charge carriers decreases with active layer thickness. That's because only charge carriers generated within some diffusion lengths to the interface of active layer and electrodes (or buffer layers) can be collected by electrodes (or buffer layers). Charge carriers generated outside this diffusion length mostly will be lost due to nongeminate recombination.[47, 48] In the literature, the charge carrier collection progress has been attributed to carrier drifting in the built-in electric filed next to interface of contact. The efficiency of this process is dependent on the ratio of drift length

$L_{dr}=\mu\tau F$ and device thickness d.[49, 50] (Let's define these symbols first here: μ is the charge carrier mobility, τ is the charge carrier lifetime, and F is the electric field.) This drift length is a good parameter to explain why charge carrier collection is thickness dependent. The electric field $F=(V_{bi}-V)/d$, where V_{bi} is the built-in voltage if the space charge in the device can be ignored. Then we can the expand ratio:

$$\frac{L_{dr}}{d}=\mu\tau\frac{V_{bi}-V}{d^2} \quad (1)$$

The expanded ratio points that charge carrier collection is inversely proportional to the square of active layer thickness. This behavior of charge collection impacted by device thickness is severe when the thickness is much larger than the depletion region thickness.

So with the active layer increasing after some value, the number of collected charge carriers decreases and causes the photo generated current to decrease. This was demonstrated in the short circuit current density curve in Figure 5b of [Dibb 2013]. The short circuit current density of fairly thick device is considerably low as observed in Figure 5b of [Dibb 2013]. The fill factor also decreases with thickness after some value due to a combination of charge combination and space-charge effects.[51]

With these limitations on device performance due to thickness, it's helpful to find an optimum thickness to get the highest device efficiency. However, it has been a challenge to find the optimum active layer thickness considering the trade off between photon absorption and charge collection. Additionally, optimum active layer thickness is different for different devices, like on different polymers, different solvents, different device structures and etc.

The optimum active layer thicknesses are usually within ~100nm or less due to low mobility-lifetime product of organic solar cells.[49, 52] The best device efficiency happens with active layer thickness close to first interference maxima (typically below 100nm).[48] Only a

small number of high mobility polymers (like P3HT) blended with PCBM can use increased absorption at the second interference maximum (typically between 200 and 250nm).[53-56] There can be 20% to 40% of photon flux lost from incomplete absorption in other polymers due to inferior electronic properties.[51, 53, 57-61] In an OPV device, only a small region of the solar spectrum is covered. For example, a bandgap of 1.1 eV is required to cover 77% of the AM1.5 (air mass) solar photon flux (assuming complete absorption of the solar emission intensity by the material), whereas most solution processable semiconducting polymers (PPVs, P3HT) have bandgaps larger than 1.9 eV, which covers only 30% of the AM1.5 solar photon flux (assuming complete absorption of the solar emission intensity by the material) as shown in Figure 1b of [Li 2012].[62] If the thickness of the active layer (P3HT:PCBM) is limited to ca. 100 nm, results in an absorption of only ca. 60% of the incident light at the absorption maximum (without back reflection of the electrode).[45]

Hence, to boost efficiencies further, it is imperative to reduce optical losses and improve light absorption within existing OPV architectures. Designing new donor polymer with smaller bandgap would be a way to increase light absorption by broadening absorption band. However, searching for a new donor polymer which has a relative small bandgap and high carrier mobilities is not easy and takes a lot of try and experiment. There are more requirements as well to the donor polymer like having good mixture with acceptor fullerene, not having too many defect states in the bulk and interface, and etc. We need to search for alternative approaches to reduce optical losses.

2.2 Photon Management Methods in OPV Devices

So approaches in optical aspect, like increasing photon flux within device should be reached out as an alternative method. An increased photon flux can be obtained in several ways, like by concentration of the light, light trapping or using photon recycling.[63] Let's look closely at the light interaction with device. In a normal solar cell, light is incident at normal concentration and light can be escaped from absorbing by reflection and transmission. This amount of escaped light contributes to the optical losses.

2.2.1 Antireflection Coating

One simplest way to increase absorption is to reduce reflection using anti reflection (AR) coating. AR coat has a dielectric thin film with refractive index n_d intermediate between air (n_0) and semiconductor materials (n_s). According to the reflectivity equation[63], reflectivity disappears when n_d equals the square root of $n_0 n_s$. If we assume refractive index of air space is 1, by having an AR coat with refractive index equaling square root of refractive index of semiconductor materials, the reflectivity can be reduced to zero at some particular wavelength. It's better to choose the wavelength in the middle of the absorption spectrum. However, the reflectivity at other wavelengths can be high with phase shift from wavelength. In order to solve this issue, AR coat consisting of multiple layers of thin films with different refractive index can improve the reflectivity reduction at larger range of wavelengths. There are quite a few studies in search for perfect AR structure.

With a layer of moth eye anti-reflection coating (2D sub-nanometer grating structure), reflection of the substrate in organic solar cell is reduced and results in an increase of peak EQE by 3.5%.[64] This enhancement is also valid for a wild range of incidence angles and

works better in high incidence angle. Here the reduction of reflection is mainly on the cut of the reflection at the interface of air and glass.

Another reflection reduction on organic solar cell is achieved by partially spherical structure as omnidirectional AR coating.[65] Using these microstructures, near zero reflection was achieved over a large spectral region and large range of light incidence angles. In theory, there mainly exists three types of nonabsorbing omni-AR structures. One type is single or multilayer quarter-wavelength film stacks.[66] The second type is the graded index (GRIN) AR structures. [67] The third type is textured surface AR structures. [68-70]

2.2.2 Light Concentration

There's another practical method of increasing light absorption. It's to collect light over a large area and focus light on a device surface of smaller area. This approach could easily increases incident light flux density at the device surface by a concentration factor, X, which is about the ratio of the collection area and device area. The advantage of this approach is reducing the cost of solar cell from materials and fabrication. Especially most of polymers used in the efficient organic solar cells are quite expensive, which makes the manufacturing cost far from competitive in the general electricity market.[71] Concentrating optics usually are much cheaper per unit area than solar cells per unit area.

In the inorganic photovoltaic system, imaging concentrators are widely used. However, a tracking system is usually needed to follow the sun during the daily and seasonal trajectories to have concentrators pointing to sun.

Alternatives to this imaging concentrators are non-imaging, low concentration systems which don't require tracking systems. One example is compound parabolic concentrator. Another example of non-imaging concentrators is fluorescent concentrators.

For fluorescent concentrator, a refractive material is filled with fluorescent particles and will reemit photons with a controlled spectral range. The emitted light is directed to the solar cell and results in total internal reflection.

Koeppe reported using luminescent concentrator on organic solar cells from zinc-phthalocyanine and C60.[72] Using organic dyes with high photoluminescence quantum yields, luminescence concentrators can concentrate the incoming light while red-shift it and couple it to a waveguide. Luminescence concentrators helped overcome the absorption limitation below 600 nm by spectrally shifting the blue/green light toward the red light and waveguide it to the solar cell. In order to fully utilize the transmitted red light through concentrator, a second solar cell was employed. The photogenerated current density is higher than a single solar cell of the same active area, increasing from 8.5 to 10mA/cm^2.[72]

In practice, the concentration systems can increase the power conversion efficiency of high quality inorganic solar cells by a few percent. However, if this improvement from reduction in optical losses and incomplete absorption of diffuse light are weigh together, concentrator systems don't necessarily do better than one sun module in AM1.5. So concentrators are primarily for reducing the cost by reducing device area, not for improving device efficiency.

2.2.3 Photon Recycling

Another strategy to reduce optical losses is using Photo Recycling (PR). PR is to reabsorb photons that are emitted by radiative recombination inside the cell. Radiative recombination of electrons and holes in semiconductor is unavoidable, though it might be extremely small. Usually photon recycling increases with average ray path length and therefore within the realm of light trapping. Photon recycling is stronger in device with good

rear reflectivity, like devices with rear reflector. Since photon recycling only matters in materials with high radiative efficiency and all practical solar cells are limited by non-radiative processes, photon recycling is still a theoretical method to achieve higher efficiency.

The most important and popular approach to reduce optical losses and increase device performance is using light trapping techniques. Optimizing light absorption and charge carrier collection simultaneously is the goal of light trapping to achieve higher power conversion efficiency. So only if the device performance of solar cell is mainly limited by charge carrier collection, light trapping could be very useful.

2.2.4 Novel Geometries

There has been some novel geometry designed in OPV devices to improve light absorption and device performance. A fold solar cell architecture for organic solar cells can be beneficial to improve light absorption when incident light comes at an inclined angles.

Tringstedt reported making folded V shape tandem organic solar cells, which consist two planar but spectrally different cells.[6] The non-absorbed light reflected from one cell can be illuminated onto another cell, thus broaden the whole spectral absorption and trap more light. This novel structure contributes to a power conversion efficiency enhancement of a factor of 1.8 ± 0.3. The detailed device structure and materials are shown in **Fig. 9**. This folded structure helps improve power conversion efficiency in three ways. First, the folded structure makes light come at high angles and traps the light in active layer by having longer light travel path. Second, the device occupies less surface area since the cell is folded and more photocurrent generates per illuminated area. Third, the folded structure allows optical and electrical parallel or series connection of tandem or multiple banggap solar cells. This

work reported a doubling of power conversion efficiency in both single bandgap and two bandgap tandem devices with a high angle of folding structure. This technique can be easily

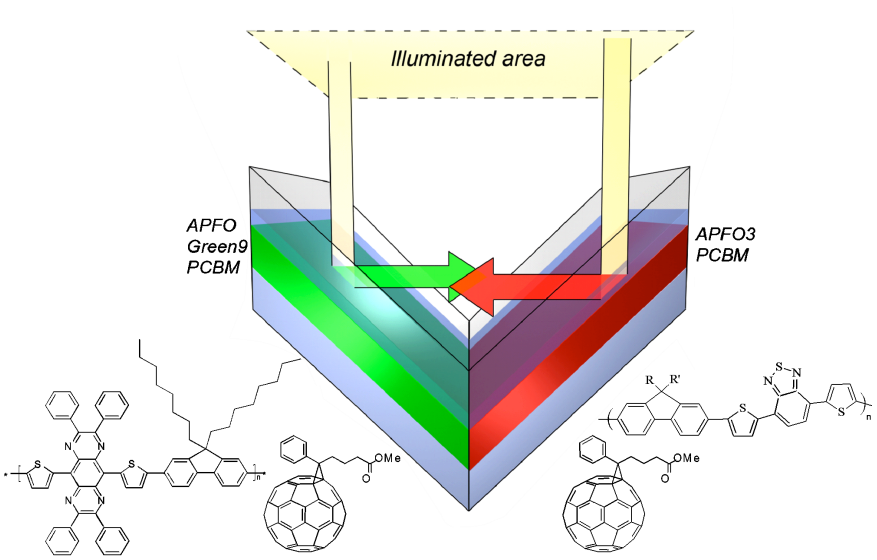

Fig. 9 Diagram of the folded V shape tandem organic solar cells.[6]

done when the substrate is plastic.

Another work with similar architecture was reported by Niggemann.[8] This structure is based on functional microprism substrate, upon which is a highly conductive polymer layer with a supporting metal grid to replace ITO electrode. This kind of architecture makes a folded solar cell as seen in **Fig. 10**. This special structure increases the light absorption in the active layer thanks to the inclined incident light and second reflection from this V shape structure. Maximum light absorption was achieved at 50^{o} incident angle for unpolarised light. Compared to a planar solar cell with 100nm thick of MDMO-PPV:PCBM, light absorption is increased by 44% with respect to solar spectrum using this maximum light absorption optimization. The dimension of this microstructure is optimized to have 120μm±35μm period and have gold grid with 20μm width. This microstructure is optimized by weighing the sheet resistivity of the polymer anode and shading effect of the metal grid. A low effective sheet

resistivity below 1**Ω/□** of metal grid was achieved by evaporating the metal grid from self-aligning through the microstructure as self-alignment mask. This structure helps increase light absorption in active layer, but there is issue with electrical shunts at the sharp tips. Further improvement in this problem needs to be addressed to obtain high device efficiency.

In addition, Niggement showed microprism better used in vacuum evaporated small molecule solar cell than conjugated polymer solar cell.[73]

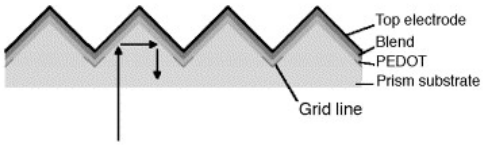

Fig. 10 Cross section of an OPV device with microprism structure.[8]

Detailed information about how to do the optical modeling of this folded structure organic solar cell can be referred in Andrsson's article.[74] The optical modeling is applied to a folded tandem solar cell, similar to **Fig. 9**. Finite element method (FEM) is used in the simulations to calculate the light absorption in both active layer and electrodes. The effect of layer thickness and folding angle on the energy dissipation was also studied and the results clearly showed the advantage of folded structure in getting light trapping. The light absorption inside active layer increases rapidly with decreasing folding angle, due to increased number of internal reflection. This increment trend is the same regardless of the active layer thickness. The enhancement factor of light absorption respect to planar cell increases with active layer thickness decreasing. Optical modeling also showed the folded solar cell have the potential to absorb more light, and generate higher mean power than equivalent planar cell during a full day with varied incident light angles.[75] This applies to both single and tandem solar cells. The simulation also showed that there is a need to consider oblique incident light when optimizing layer thickness in serial connected tandem

solar cells. Instead connecting the subcells in parallel connection is an advantage considering that factor. However, the simulation showed that the photocurrents in the folded tandem cell might be more difficult to balance by adjusting the thickness of active layer.

With the V shape structure, a successful experiment was carried out by Kim et. al on PCDTBT:$PC_{71}BM$ bulk heterojunction organic solar cell.[76] Photon absorption was significantly improved and short circuit current density increases by 29%. Power conversion efficiency was increased from 5.3% to 7.2%, a 35% improvement over the performance in the absence of a light trap. Similar findings were observed that the solar cell with V shape is always superior to the planar cell for all angles of incident light.

There are more cells based on V shape.[77, 78] The folded cells work efficiently for most incident angles, but it's difficult to realize on a larger scale since it's consuming more materials.

Besides the listed V shape architectures in organic solar cells, there are some other new designs of geometries for light trapping in organic solar cells.

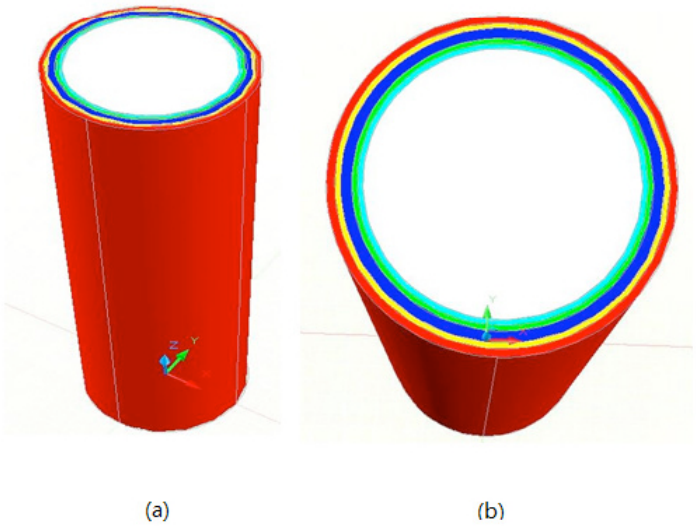

Fig. 11 Schematic diagram of OPV device structure on cylindrical glass substrate. The layers in the diagram are Al, BCP, CuPC:PCBM active layer, PEDOT:PSS, and cylindrical glass substrate.[14]

Song et. al designed a transference cylindrical substrate with light trapping structure, which is shown in **Fig. 11**.[14] In order to optimize absorption spectrum, quantum efficiency and power conversion efficiency, optical and electric simulation was carried out considering three parameters: the height, diameter of the glass substrate, and the thickness of the organic active layer. The optimum thickness of active layer for highest power conversion efficiency shifted from 65nm to 20nm. And the organic solar cell with light trapping structure on this cylindrical substrate has double device efficiency of organic solar cell with similar structure on the flat plain glass substrate. This OPV device structure can operate efficiently for light of all incident angles. So the incident angel of light almost has no effect on the device performance of this OPV device. From the simulation analysis, the best efficiency OPV would be fabricated on 5cm long and 5mm diameter cylindrical glass substrate with 20nm thick active layers.

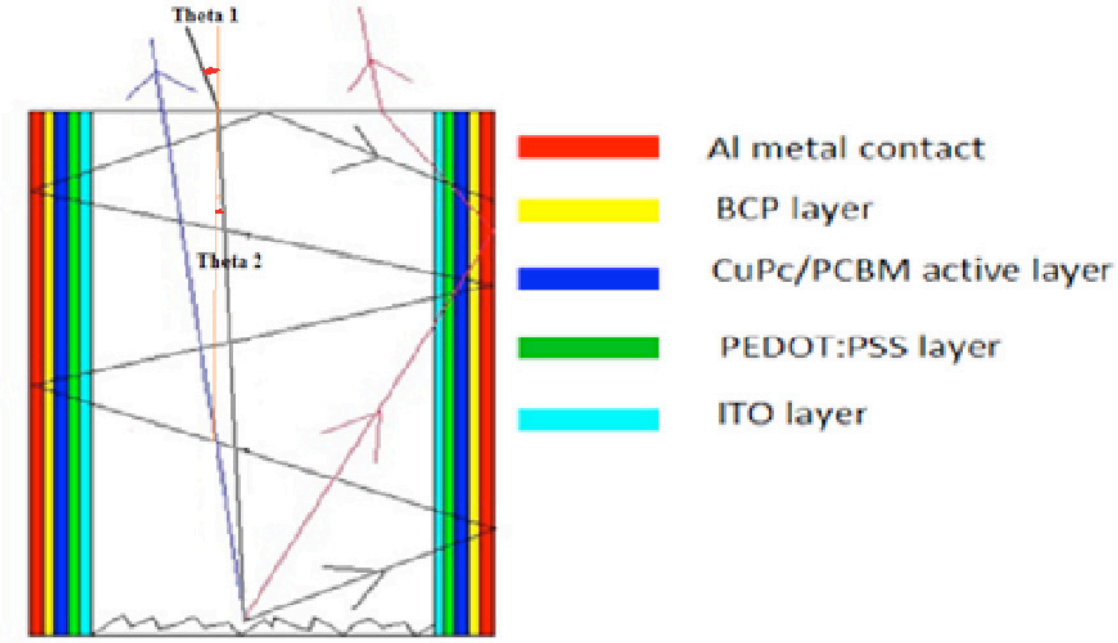

Fig. 12 Cross section view of organic solar cell on cylindrical substrate with light trapping structure.[14]

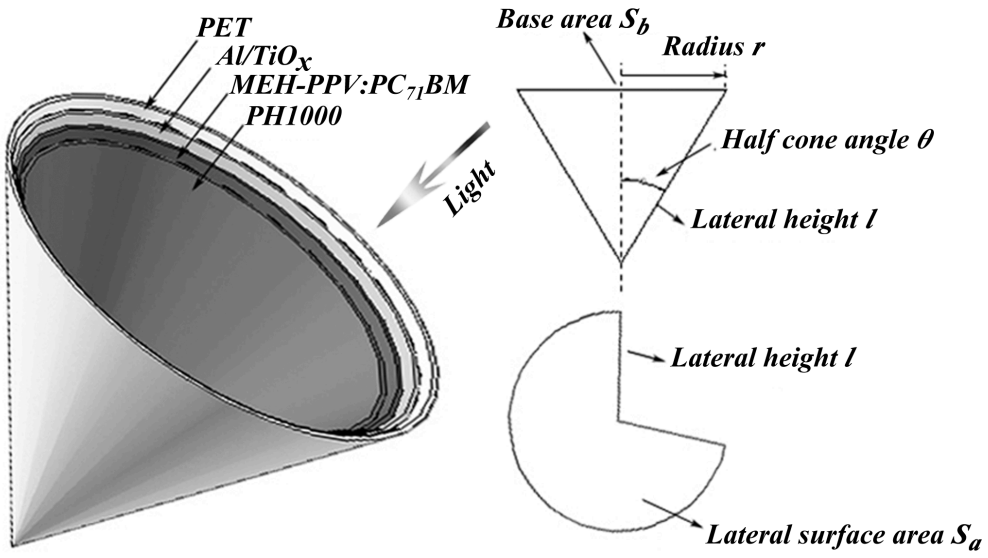

Fig. 13 Cone shape based OPV device diagram.[10]

Another novel structure-cone shape based organic solar cell was manufactured and studied.[10] The device structure is shown in **Fig. 13**. This special structure guaranteed the incident light rays are trapped and multi-absorbed in 360^{o} directions. The simulation was carried out considering two factors: wavelength and half cone angle. In the experiment, a cone shape organic solar cell with half cone angle of 45^{o}, increased light absorption by 43% than planar organic solar cell. Besides the effective light trapping, this cone shape OPV has high stability in bending shape.

2.2.5 Front Surface Coupler

Another strategy to reduce optical losses and increase device efficiency is to modify the device front surface or even induce another textured structure to the front surface.

A layer of PDMS thin film was reported to be deposited onto the glass surface of organic solar cell as seen in **Fig. 14**.[22] Random textured and V-grooved textured structures on front surface of PCDTBT:$PC_{71}BM$ bulk heterojunction solar cell were experimented and studied, respectively. The textured structures help increase optical path travel length of

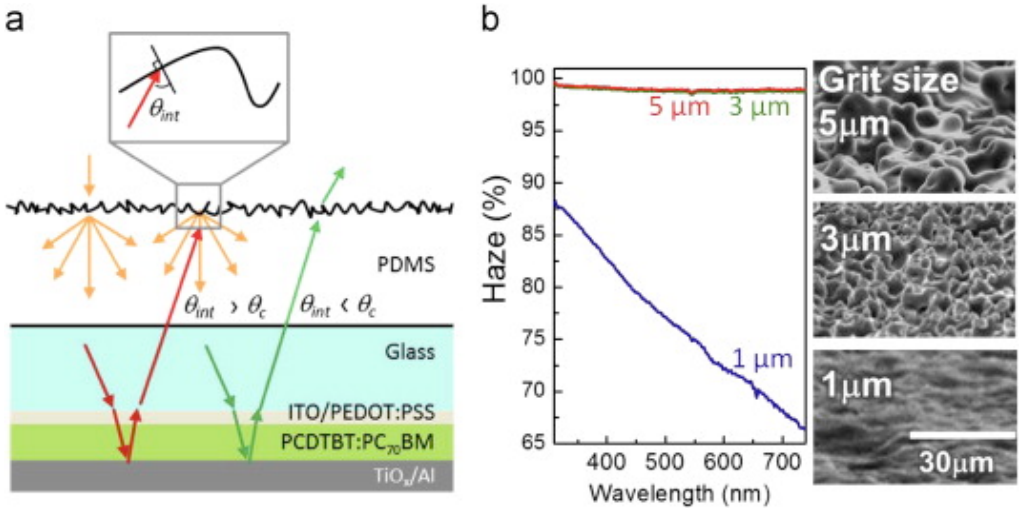

Fig. 14 Schematic diagram of OPV device with scatter layer of PDMS on glass side.[22]

incident light and trap light spectrally. Random textured structure can have an improvement of the light absorption close to that of Lambertian scatter. Experiment showed an enhancement up to 9.3% in short-circuit current density. V-groove textured structure seems to have a controllable improvement for the device efficiency by designing the dimension of the structure. It's found that V-groove textured structure with vertex angles between 100.8 and 112.0^o provides the highest enhancement as it reduces the light escaping from the structure. The choice of using highly reflecting Ag electrode also helps increase light absorption. With the optimal vertex angle for the V-groove texture structure, the short-circuit current density of organic solar cells increases by 15% and the power conversion efficiency increases from 6.5% to 7.4%.

Another structure with retroreflective light trapping texture was used on organic solar cell.[17] The structure with its geometry graph is shown in **Fig. 15**. This retroreflective textured sheet was made by a simple replication technique to transfer the structure from a

stainless mold to cross-linked PDMS. On the top surface of this sheet, there residents an array of tilted cubic structures, each of which has a size of several hundredths of micrometers. This foil sheet is flexible and can be easily applied to the glass substrate of organic solar cells. When the incident light rays hit the textured structure, they are scattered and coupled into the cell, thus increasing the incident light path length. The light reflection at the air/sheet interface is reduced from recoupling into the cell. Incomplete light rays that are reflected back to texture structure from cell are reflected back to cell. The combination of longer light

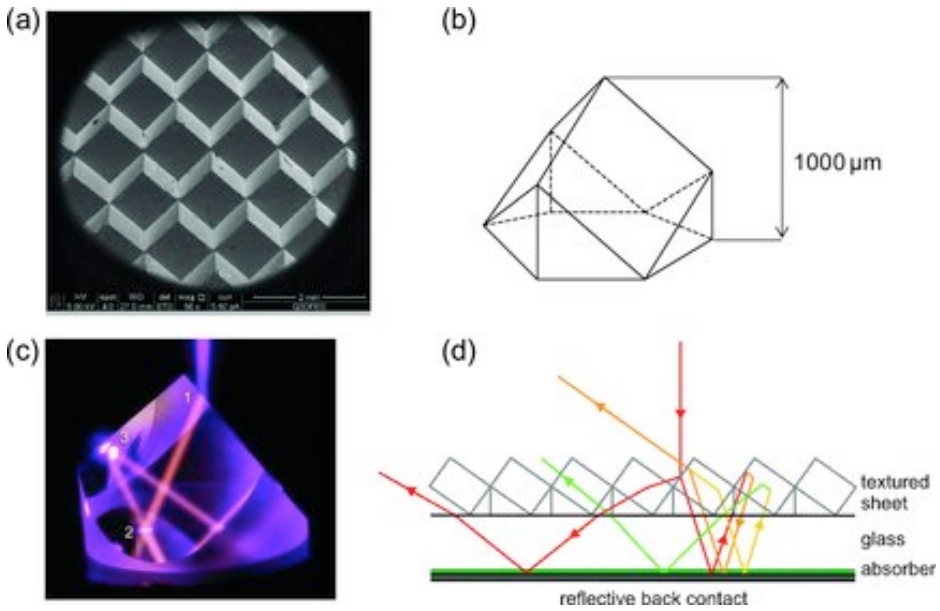

Fig. 15 A periodic texture structure and its use on organic solar cell.[17]

path and multi-absorption combines increasing light absorption in the cell. With this texture structure on PDPPTPT:PCBM bulk heterojunction organic solar cell, the EQE, photo current density of this cell is higher than the cell without this texture structure. There has seen 19% enhancement in power conversion efficiency as shown in this study.

The advantage of these external textured structures is that they don't interfere with integrity of the internal device structure.

Another similar textured structure was employed on organic solar cell as seen in **Fig. 16**.[15] However, the difference is that no external structure was attached to the front surface, but the front surface was modified to be textured structure at the interface between front electrode and buffer layer.

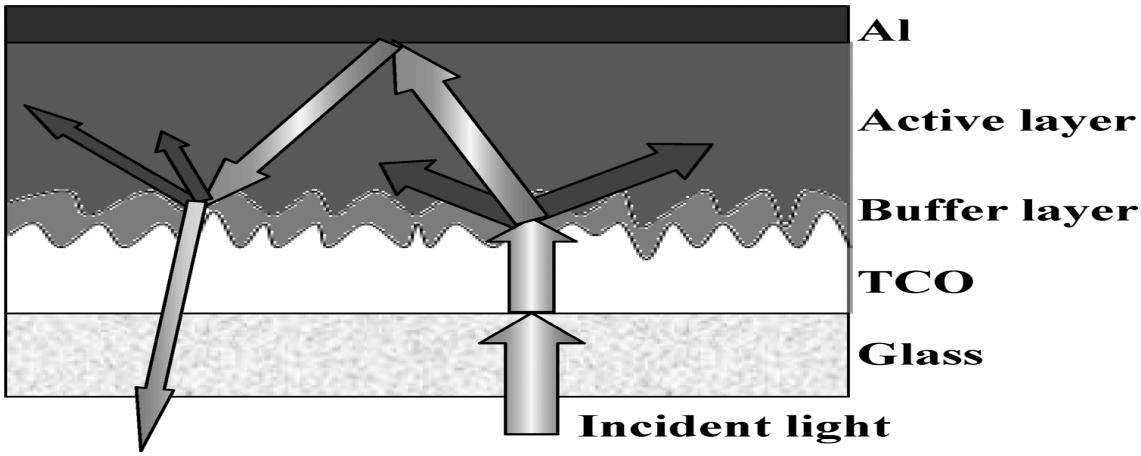

Fig. 16 Cross section view of organic solar cell on grating structure.[15]

Besides the textured interface, the reflective back electrode also contributes to the light trapping. The textured interface helps scatter incident light and reflect light from back electrode to increase light path length. Device efficiency was improved through the light trapping. This study also investigated the effect of different morphologies of the textured interface on the device performance. There were two slightly different shapes of the textured interface in the study: U shape and V shape. The enhancement of short circuit current density was 9% and 6% on P3HT:PCBM bulk heterojunction solar cells, respectively for U shape and V shape, compared to flat device. The U shape was able to form a conformal coating of buffer layer.

Another interesting structure configuration on the surface organic solar cell was introduced.[4] The structure configuration consists of an array of microlens, a highly reflecting

mirror with a self aligned array of micro apertures on it, and a optical spacer layer on the glass substrate of organic solar cell. The detailed diagram of this structure system and device is shown in **Fig. 17**. In order to get the desired microlenses, concave microlenses are generated first from controlled isotropic etching into a Cr covered quartz substrate. By imprint lithography in a malleable optical polymer resin on a glass or plastic substrate, an array of microlenses are obtained. There's a metal layer on the other side of the microlenses. The UV exposure through these microlenses generated a pattern on the metal layer and was lifted off to produce an array of apertures. With this series of optical structures, the incident light got bounced inside the active layer of the organic solar cell. There's an enhancement of light absorption and as high as 25% improvement in short circuit current.

However, this approach of using array of lenses and holes only works when the angle of incident light is in a small range.

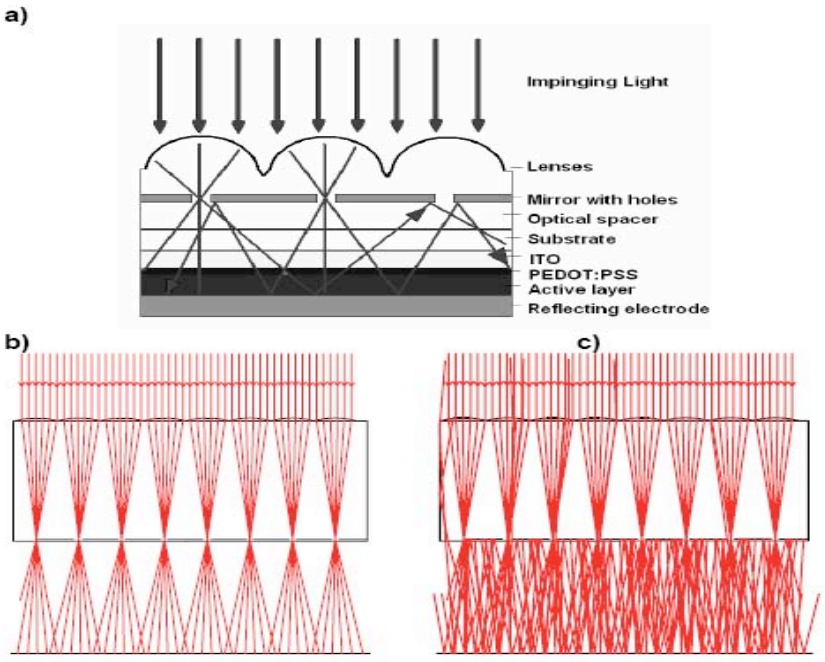

Fig. 17 Microlens structure system on organic solar cells.[4]

2.2.6 Textured Substrate

Using periodic grating to increase optical pass length, thus increasing light absorption is already commonly used in silicon solar cell. [79, 80]

Kanwar's textured substrate provides a way to fabricate efficient organic solar cell with conformal coating of active layer.[12] The grating-type textured substrates need to have dimension of sub-micrometer height (like 300 nm) and several micrometer periodical width (like 2 μm). With the grating substrate of this dimension, P3HT:PCBM based BHJ solar cell develops a 100% enhancement in average light absorption near the band edge due to trapping of longer wavelength photons. There's a 20% improvement in PCE compared with the flat solar cell.

Another previous study by Niggemann used similar grating structure like here, but failed to deliver a conformal active layer. In Niggemann's work, two cell architectures-diffraction gratings and buried nano-electrodes were investigated.[19] The diffraction grating structure was imprinted from the master structure, which was made by holographic exposure of photoresist coated glass substrate. Though this diffraction grating helps increasing absorptance in the active layer in TE-polarization by 15.3%, there's a reduction of 32% in absorptance of TM-polarization. This high loss in TM-polarization could be due to the corrugation of the metal interface. Another buried nano-electrode structure has a dimension with period of 720 nm, depth of 400 nm and width of cavities at 400 nm. Metal electrodes were evaporated into the bare nano structure at certain angles to make sure the bottom of cavities were enough transparent. Following MDMO-PPV:PCBM/PEDOT/Au layers were deposited onto this buried nano-electrodes. The device has electrical performance with short circuit current density of 2.5 $mAcm^{-2}$ and open circuit voltage of 550 mV and fill factor of

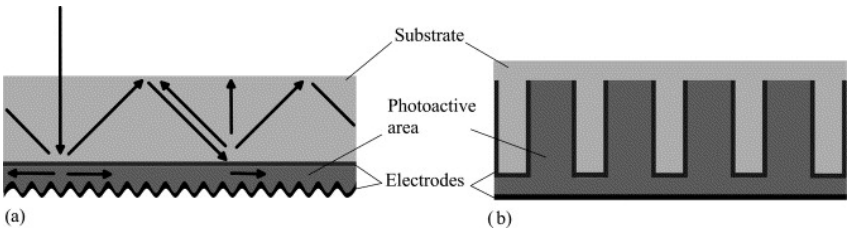

Fig. 18 Two architectures in OPV: (a) diffraction gratings; (b) nano-buried electrodes.[19]

only 25%. This low efficiency is due to non-conformal coating of polymer layers on the nano-strucutre, which leads to air gaps in the middle of cavities and shunts at the corner of pillars. The dimension of this structure, which results in non-conformal coating, can be optimized to have conformal coating as discussed in Kanwar's experiments.

In Kanwar's paper, Kanwar argued that the design of this grating structure should not be solely decided by having the best optical design. In the case of building thin film organic solar cell on the grating structure, the quality of having conformal coating and thus high electrical characteristics is more important. The proposed device structure with textured grating is shown in **Fig. 19**. The bottom 1D photoresist grating was formed by soft lithography from a pattern master, which was made from laser interference lithography. In order to obtain a proposed conformal polymer layer on grating structure, gratings of several different dimensions were investigated. When both the period and height of the grating structure are greater than 1 μm, the deposition of active layer showed non-conformal coating. In the middle of the valley, there are air gaps and film is underfilled. While on top of the gratings, the active layer is much thinner than that in the valley. This spatial difference of active layer thickness could create unbalanced photocurrent spatially. The possible shunts at the top corner of the gratings further deteriorate the electric characteristics. With height of grating is reduced to sub-micrometer (300 nm here) and period of grating close to 1 μm, the conformal coating of active layer on the grating was improved. There were no air-gaps and

shunts. However, there was thicker active layer in the middle of valley than that on the grating. This kind of overfill can result in more recombination losses. When the period of grating was increased to 2 μm while the height was kept the same, the active layer had a fairly conformal coating with respect to the topography of the grating substrate as demonstrated in SEM and AFM. As expected, the electric characteristics of OPV devices on the first and second grating substrates were not as good as devices on grating substrate with dimension of 2 μm period and 300 nm height. The airgaps and shunts affect the open circuit voltage and fill factor. And the overfill could reduce all the electric characteristics due to more recombination losses. More about the light trapping can be seen in the article.[12] However, the requirement of getting an appropriate aspect ratio and conformal active layer coating brings hurdles to scale this technology and expand its use to other solar cell systems.

Surface textures traditionally were made by lithography from photo resist coating, exposure and transfer processes[81] or printing, moulding and embossing approaches.[82, 83] Many have used electron beam and ion beam lithography to produce precise grating structures. Here another similar surface texture was obtained by direct laser interference patterning (DLIP).[21] This technology was used here to produce large area of two-dimensional periodic surface patterns on polyethyleneterephthalate (PET) substrates. The structure of this texture can be seen in **Fig. 20**.

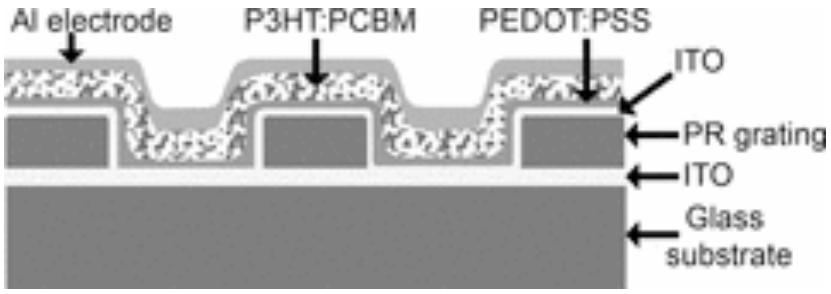

Fig. 19 P3HT:PCBM OPV device on textured structure.[12]

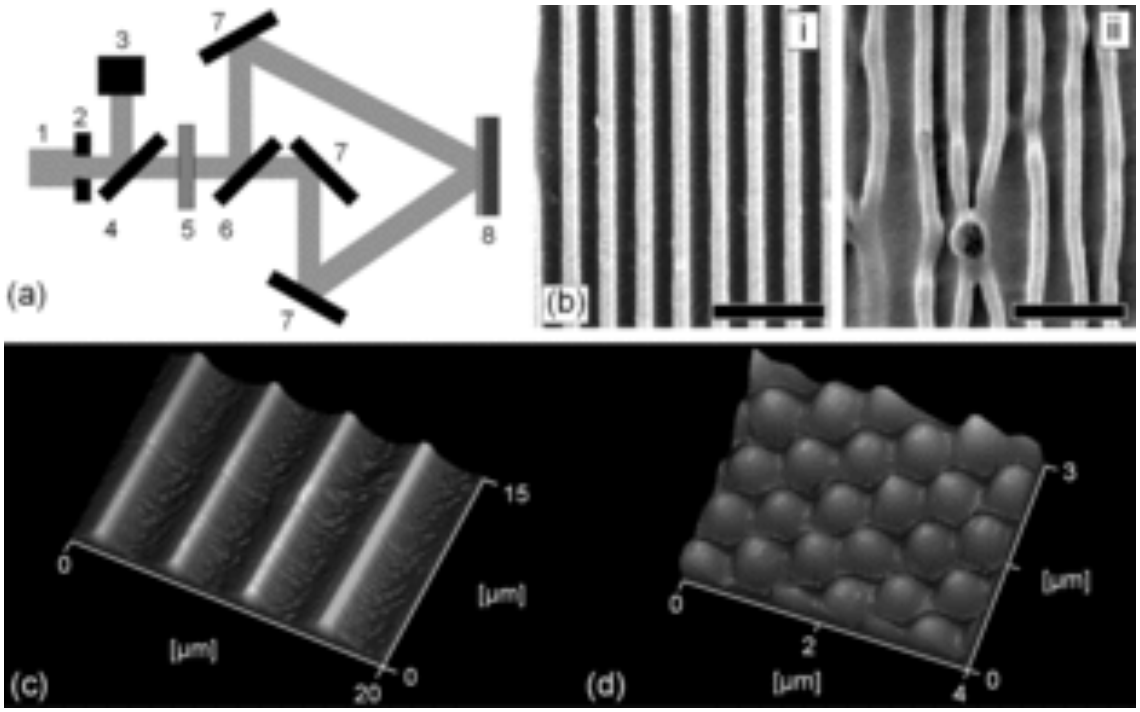

Fig. 20 Nanowire shape of textured structure.[21]

Here two dimensions of surface textures were fabricated with one of period 0.7 µm, height 140 nm in line shape and another of period 4.7 µm, height 735 nm in hexagonal shape, corresponding to aspect ratio of 0.19 and 0.15, respectively. PEDOT:PSS and ZnPc:C60 layer were deposited later on the surface texture. The OPV device with surface texture showed higher device performance than that without surface texture. To explain the reasons of this performance enhancement, the authors brought up several mechanisms. Light trapping definitely is one of them to contribute to the performance enhancement. However, after comparing the device enhancements from the surface textures of two different dimensions, small difference in the two enhancements was found which indicates that light trapping is not the main factor. The mechanism of diffraction into waveguide modes was also excluded from the main factor. The mechanism of elongated optical path on a tilted surface, smaller effective thickness of active layer on the substrate slope, and better absorption caused by surface plasmons on the silver back reflector were also ruled out from the main cause. The

main cause of the device performance enhancement was attributed to the reflection on the curved surface and diffraction by the periodic structure.

Another grating inside the device: using ordered 2D-dot nano-patterned anode in organic solar cell as seen in **Fig. 21**.[18] This well-ordered nano structure was fabricated from nanoimprinting technique to form a patterned conduction IZO film. This patterned IZO layer has 50 to 200 nm height and 265 nm period. Organic solar cells based on IZO, PEDOT:PSS, P3HT:PCBM, and Al were fabricated. The organic solar cell with this textured anode has better performance than that with flat anode. Short circuit current density was increased from 7.03 to 8.94 mA/cm^2 and PCE was enhanced from 1.05 to 1.71%.

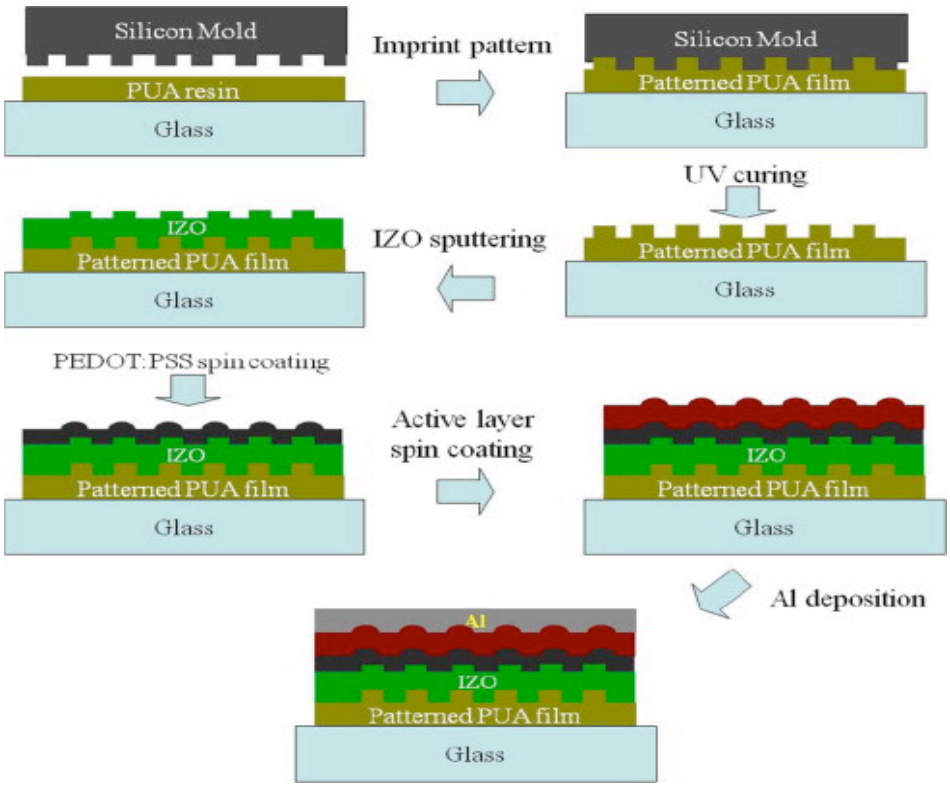

Fig. 21 Schema of fabricating textured anode and organic solar cell.[18]

The performance enhancement is due to large interface area between electrodes and active layer, enhancing more photogenerated charge carriers collected by electrodes. Light trapping

and scattering of reflected light help increase light absorption and contributes to the performance enhancement.

For these methods using textured structures on the top surface of the solar cells, some can be directly integrated into the device layers, mainly into the electrode layers. Some methods are separating the textured structure from the device layers, or inserting an optical spacer layer between texture layer and device layers to avoid inducing electric defect onto the device.

Other works on using textured substrate can also been seen in other references. [84] [85] [86] [87] [21]

2.2.7 Structured Back Reflector

The other similar approach is to attach an external structure at the back surface of solar cell. Tang et. al used a layer of dielectric scatterer at the back substrates of single organic solar cell and tandem organic solar cell.[88] The dielectric scatterers are mixture of TiO_2 nanoparticles and PDMS. The optical characteristics can be tuned by changing the TiO_2 concentration. A dielectric scatterer layer with reflectance close to 100% at wavelength longer than 400 nm can be achieved. In the semitransparent organic solar cells, where optical loss is a big limiting factor of power conversion efficiency, this dielectric scatterer layer was put at the back of device substrate. The device structure of this organic solar cell is glass/PEDOT:PSS/Active layer/ITO/glass substrate/Dielectric scatter. The active layer is the bulk heterojunction layer of TQ1 and $PC_{71}BM$. The normal organic solar cell without dielectric scatterer has a short-circuit current density of 5.5 $mAcm^{-2}$, and power conversion efficiency of 2.7%. Using the dielectric scatterer with reflectance close to 100% at larger than 400 nm, there's an improvement of short-circuit current density by 80%, and the PCE is

improved to 4.6%. In contrast, by replacing this dielectric scatterer layer with planar silver mirror layer, the device only has an improvement in J_{sc} of 45%, less than the effect of dielectric scatterer. Since the reflectance of silver mirror and dielectric scatterer are not that different, the higher device improvement from dielectric scatterer is due to light trapping effect. An interesting study of this work is to study the enhancement effect with different electrode thicknesses. It's found that the reduction on device performance is larger with dielectric scatterer when increasing the thickness of PEDOT:PSS. This indicates that the parasitic absorption from electrodes can limit the benefits from dielectric scatterer. The enhancement from dielectric scatterer increases when the thickness of active layer decreases. This makes sense, as the device would benefit more from this light trapping structure when more optical loss is expected from thinner active layer. The reflection loss can be 20% spectrally even the device with dielectric scatter is optimized. Mostly the loss is from glass reflection and escaping of light reflected from dielectric scatterer with a small angle of incidence angle. In order to keep reducing the reflection loss, tandem solar cell is employed. Parallel tandem organic solar cell with the same cell of TQ1:$PC_{71}BM$ is shown to have improvement of 32% in J_{sc}. A tandem organic solar cell in serial configuration was also investigated. In order to get a balancing photocurrent between these two subcells, a dielectric scatterer layer was sandwiched between TQ1 and P3T1 based subcells. The photocurrent balancing can be easily adjusted by changing TiO2 concentration or thickness of dielectric scatterer. As a result, a series tandem organic solar cell with 7% PCE is achieved with the help of dielectric scatterer.

Most of these back reflectors are achieved by modifying the existing electrodes to have diffraction gratings. These diffraction gratings help couple the reflected light into

waveguide modes to increase light absorption. These modifications are usually done using soft lithography imprinting techniques.[1, 19, 89-91]

A periodic sub-micrometer structure-surface relief grating (SRG) was achieved by imprinting PDMS as stamp on the active layers, which is from the masters of photoresponsive azo polymer films.[91] Different from photolithographic processes, the technique to pattern polymers used here is a damage free process. The choice of using azo polymer as the master has several benefits, including a one step process, feasible duplication, easy to control grating profile, easy of fabrication, and ability of superimposing multiple patterns. A grating structure with period of 500 nm and height of 20 nm was fabricated. Organic solar cell in structure ITO/PEDOT:PSS/P3HT:PCBM/Ca/Al was fabricated with one metal electrode Ca/Al flat and another pattern by the grating structure. It's demonstrated that the increase in the optical path by diffraction of light can be obtained in a broad range, especially in the important light absorbing region of P3HT:PCBM based OPV. The electric characteristics showed the OPV device with SRG has 0.62 V V_{oc}, 10.5 mA/cm^2 J_{sc}, 63% FF and PCE of 4.11%, higher than OPV devices without SRG with 0.61V V_{oc}, 9.45 mA/cm^2 J_{sc}, 61% FF and 3.56% PCE. Most of the enhancement is from the improvement in the J_{sc}, instead of V_{oc} or FF. This means that SRG can help increase phtogenerated charge carriers by more light absorption inside active layer from the increased optical path length and light trapping. The effect of period, depth and dimension of the gratings on the performance of organic solar cell were further investigated in another continued report.[90] Here 2D SRGs were fabricated besides 1D SRGs by having one more exposure to 1D SRGs after rotating 90^o. The 1D SRG pattern has a period of 500 nm. The 2D orthogonal cross-grating pattern also has a period of 500 nm. The period and height of the SRGs can be tuned by the incident

angle and irradiation time of the interfering Ar^+ laser beams, respectively. Organic solar cells with SRGs at period of 500 nm and grating depths of 10 nm, 20 nm, 30 nm and 40 nm were made and compared with organic solar cell without SRG. Only cell with grating depth of 40 nm didn't improve cell performance. Cells with SRGs of other grating depths all showed enhancement to device efficiency. Cell with grating depth of 20 nm has the highest efficiency. Increasing grating depth from 20 nm to 40 nm, there's an increase in series resistance, reduction in shunt resistance, which leads to reduction of FF. In order to study the effect of grating period on device performance, SRGs with grating depth of 10 nm and periods of 300 nm, 400 nm, 500 nm, and 700 nm were made and incorporated into organic solar cell. The electrical characteristics of devices with these SRGs and reference cell without SRG were compared. Values of J_{sc} and PCE in cells with SRGs were all improved. The cells with SRGs periods of 300 nm, 400 nm, and 500 nm have similar PCE. However, the PCE enhancement from cell with SRG period of 700 nm is less than that with 500 nm periodic SRG. This can be explained as smaller period can bend light in a larger angle and increase the optical path length, resulting in higher cell efficiency. Structures of 1D SRG and 2D SRG with the same dimension were also investigated and applied to the P3HT:PCBM based organic solar cell. Electrical characteristics of these cells showed higher device performance in devices with SRGs than reference cell. Moreover, cell with 2D SRG has higher J_{sc} than that with 1D SRG, which contributes to higher device efficiency in 2D SRG device. This experimental result is consistent with the theory.[92] This is due to enhanced diffraction intensity in the broad wavelength range for the cell with 2D SRG.

Another one-dimensional periodic patterning was used at the back electrode of a copper phthalocyanine:C60 heterojunction solar cell.[84] The periodic structure was fabricated

by a single step all-optical technique based on photoinduced mass transport in azo polymer film. One of the conventional methods that were studied to make periodic structures is photolithography. However, the drawbacks of these techniques are having solvents or exposure to UV in the fabrication process. This could harm the optical and electric characteristics of the active layers in the solar cells. There have been some other techniques developed in the recent years to realize periodic structures while avoiding the drawbacks mentioned above. Soft lithography technique is one of them. In this work, an all-optical patterning structure was used to make surface microstructures on azo polymer films. Using interference patterns from the superposition of two coherent light beams, this periodic structure was realized onto the film. The period of the grating is decided by the angle between incident light and the film surface. The modulation amplitude of the grating (or called depth) is controlled by the energy hit on the film surface. Onto this grating substrate, films of azo dye molecule [4-(N-(2-hydroxyethyl)-N-ethyl-)amino-4'-nitroazobenzene]/poly(methyl methacrylate) (co(DR1/MMA)) layer, silver layer, ITO layer, PEDOT:PSS layer, CuPc/C_{60}/BCP layer and silver layer were deposited on one another. EQE measurements were carried out to investigate the effect of grating dimension on device performance. Current-voltage measurements also showed performance improvement from grating structure. All of these are due to improved absorption from coupling light inside layers through diffraction onto the patterned surface.

Another work reported using functional light trapping nanostructures on flexible substrates to improve light absorption for organic solar cells.[1] It was found that the gratings with 500 nm pitch size gave the highest light trapping efficiency for P3HT:PCBM based organic solar cells. Enhancement of power conversion efficiency as high as 34% was resulted from this kind of grating structure. The technique mentioned here successfully achieved

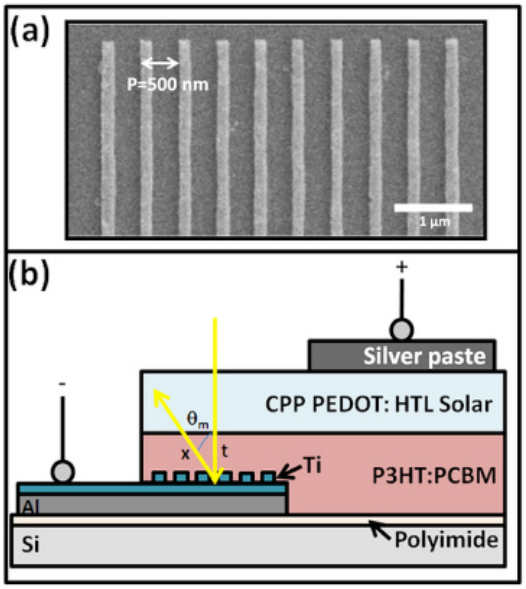

Fig. 22 SEM of grating structure and cross section of organic solar cell.[1]

nano-metric grating structure on flexible substrates. There are other techniques like laser patterning to fabricate light trapping structures on flexible substrate, but have limits like small feature size. The method used here employed polyimide thin films since polyimide films can be easily handled on the supporting substrate and are compatible with both electron beam lithography and photolithography processes. Grating patterns with 100 um x 100 um were fabricated on the back electrode of P3HT:PCBM based organic solar cells. The device structure can be seen in **Fig. 22**.

The silicon support substrates were peeled off from the cells to make flexible cells. The light trapping effect was also studied in the reflectivity spectra. The overall reflectivity is smaller in device with gratings than the flat device. This corresponds to higher absorption in device with gratings than the flat device. The study of devices with gratings of different dimensions showed that device with 250 nm gratings has lower efficiency than flat device. This indicates that inappropriate design or inferior dimensions of gratings would in fact reduce device performance. One has to be careful when designing the gratings for organic solar cells to exploit the advantage of light trapping.

Another work reported P3HT:PCBM based organic solar cells on random textured substrate from nanoimprinting technique. This texture is stamped from textured Si wafer under room temperature. There has been enhancement in J_{sc}, V_{oc}, FF and PCE for devices, among which FF contributes to most of improvement. Introduced here, applied pressure is also found to give to the enhancement of device performance. Several works reported improved charge mobility and PCE from hydrostatic pressure in pentacene based small molecule solar cells.[93-95] The imprinting increase surface roughness. Another effect from the imprinting is that P3HT became more ordered as observed in dark IV measurement and Raman spectra.

Another textured structure at the back electrode of solar cells is formed on the surface of active layer from imprinting.[20] This process was done using commercially available anodic aluminum oxide (AAO) membrane filter. The AAO mold has about 200 nm feature size. The imprinting shapes the active layer surface and increases the roughness. Higher ordering of P3HT was measured using GIXRD and contributes to higher efficiency of hole transport in P3HT. The textured interface between active layer and back electrode

scatters incident light in the active layer and increases light absorption. All these benefits help P3HT:PCBM based organic solar cell increases PCE from 3.52% to 4.43%.

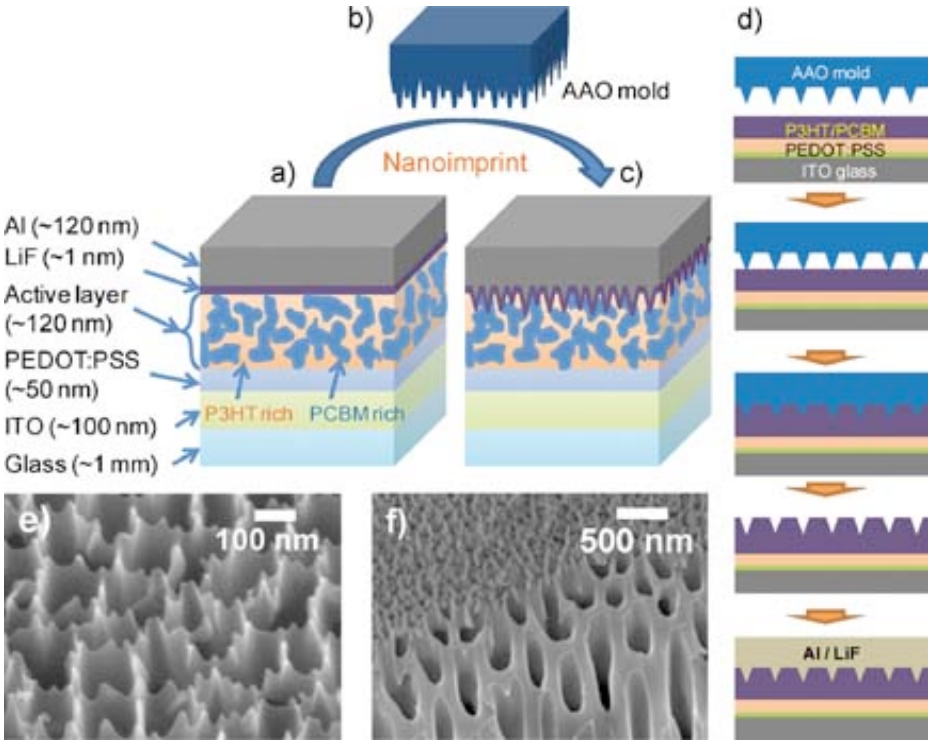

Fig. 23 Diagrams showing the fabrication of organic solar cells with textured back reflector.[20]

Another report with back reflector to induce light trapping effect in active layer tried a pyramidal structure.[13] The pyramidal grating was fabricated by molding a transparent polymer on planar substrate. It has base angle of 30°. The visual structure can be seen in **Fig. 24**. With this pyramidal grating structure, the light path length inside active layer was increased by more than 2.5 times, superior to planar rear reflector. Electrical characterization showed photocurrent enhancement between 11% and 75%, depending on the device size and active layer thickness. This is due to multi-absorption of incident light, possibly four passes after reflection from rear reflector and total internal reflection at the original incident light

interface. This structure has another advantage that it doesn't alter the active layer structure since it's applied on the top of the surface as a mold.

Here is another work to use grating structure to increase light absorption by trapping light effect.[9] This article suggested that the original optical designs for inorganic solar cells can't be directly transfer to solution based organic solar cells. Since the organic solar cells usually have active layers around 100 nm thick, which needs the scattering element pretty close to cells or in direct contact. However, the scattering element is preferred not to in direct contact with active layer to avoid any electrical defects. Another issue with light trapping structure direct contact with active layer is that the surface recombination would be increased as the surface to volume ration increases. This work used a large titled reflective structure to direct light into TIR angles in the ray domain. Other light trapping structures that work in the wave domain include blazed grating, holographic, and others

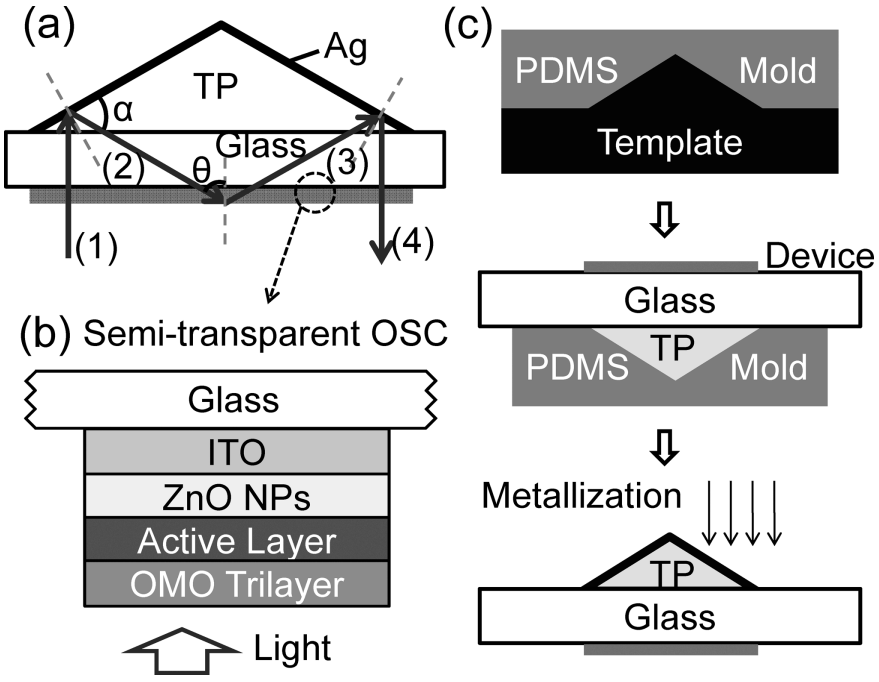

Fig. 24 Cross section of pyramidal structure and organic solar cell device.[13]

using multimodal waveguide coupling from diffraction of fine structured patterns. The structure used in this work is similar to an array of tilted mirrors, with pitch size of 55 μm and height of 40 μm. The reflection of light at the inside of dielectric media is better than that in the metals due to the complete lossless. Since most of optical losses are due to transmission instead of reflection as in conventional inorganic solar cells, semitransparent solar cells with well reflective structure at the rear are needed. This diagram of this structure can be in **Fig. 25**. As illustrated in the figure, reflecting structures are on the substrate. There is a layer of optical spacer on the reflecting structures. On top of optical spacer layer, normal organic solar cell are deposited with multiple cells aligned. Glass (or plastic) is used as highly transparent encapsulation lid on the cells.

However, the expected enhancement here is lower than the Yablonovitch limit ($4n^2$)

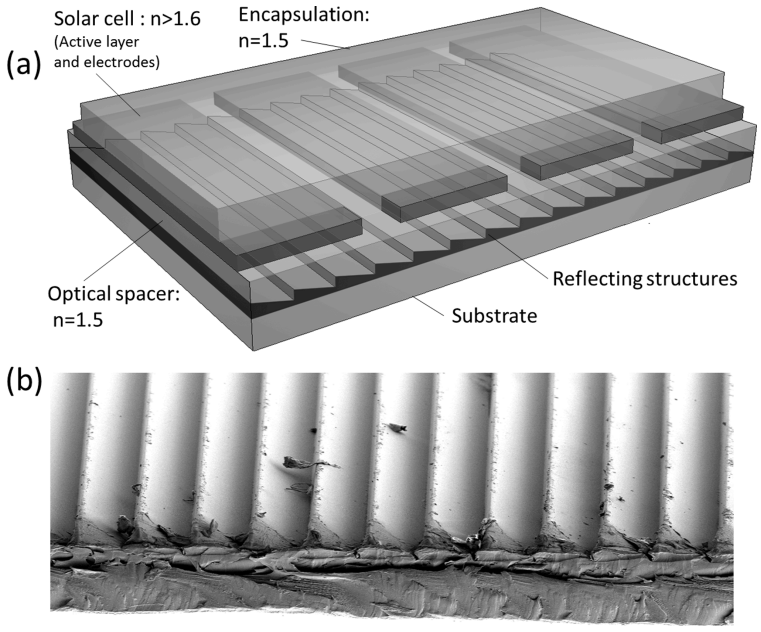

Fig. 25 (a) Device schema with reflecting structure (b) SEM images of grating structure on substrate.[9]

for light scattering under such perfectly randomizing conditions. This is not as ideal as a Lambertian reflector. Absorption measurement with TQ1:$PC_{71}BM$ active layer showed the highest absorption in cells with this reflective structure, higher than cells with flat reflector. Comparisons among cells with this reflective structure, planar reflector and no reflector were made in measurements of EQE and IV. Cells with this reflective structure all showed the highest performance. It's noticed that cells with reflective cells have 24% higher photocurrent than that with planar reflector. Angle measurement of simulating the full day illuminations also showed enhancement from the reflective structure.

However, as pointed out in the above paper, the metallic reflector has parasitic absorption, which would limit the enhancement of light absorption in the active layer. Using dielectric scatter instead would help solve this drawback. The implementation of using dielectric scatters proves this claim.[88]

This grating leads to enhancement in short circuit current density and PCE of P3HT:PCBM based organic solar cell, demonstrating the light trapping effect from this grating structure.

2.2.8 Plasmonic Methods

Another important strategy to help trapping light in organic solar cells is using plasmonic effects. This effect basically is collective oscillations of free electrons at metal-dielectric interfaces. The free electrons can be either inside metal nanoparticles or at the metal-dielectric interface. The excitation of these free electrons can help reserve energy in two modes: localized surface plasmon resonance (LSPR) in the nanoparticles, and surface plasmon polaritons (SPP) at the metal-dielectric interfaces. This type of energy storage can be converted to absorption in the active layers through either near field effect or far field

coupling. Corresponding to the two types of energy storage, two types of plasmonic structures are usually applied in organic solar cells: surface plasmon polaritons and nanoparticle plasmons.

Usually there are three ways of increasing light absorption using plasmonics. First, light can be scattered by metallic nanoparticles to be coupled and trapped as propagating plane waves inside the photoactive layer. Second, plasmonic near-field can be created around metallic nanoparticles as subwavelength antennas so that the effective absorption cross-section can be enlarged. Last, nanostructures near metal-dielectric interface can help couple light into SPP modes and guides modes to convert light into more carriers. Let's look in details of these plasmonics methods.

2.2.8.1 Light Scattering Using Particle Plasmons

The strategy of embedding metallic nanoparticles in the homogeneous layer gives a nearly symmetric light scattering in either normal or inverted device structure.[96] However, there's still some slight difference when the nanoparticles are placed close to the interface of dielectrics. The light tends to be scattered toward the dielectric with higher permittivity.[97] With light scattered from the particles, the light will be spread wide at some angles, which increases the optical path of light. Light rays with spreading angles larger than critical angle continue to be trapped inside the cell, contributing to more light absorption. With metal layer at the back of the cell, unabsorbed light will be reflected toward the surface and got scattered again while encountering the particles again. All of these actions will help increase the optical path length by several times.

The history of using the metallic nanoparticles for plasmonic effect to couple light into semiconductor layer can be dated back to late ninth. Stuart and Hall succeed coupling

light into Si-on-insulator photodetector structures with dense nanoparticles arrays as resonant scatters.[98, 99] Not until twenty first century that this technique was used in thin film solar cells to help trap light. Applications of this technique in thin film solar cells of different material systems can be learned in different literature studies, like in single crystalline silicon,[100] amorphous silicon,[101, 102] Gallium Arsenic.[103]

Even though this technique is experimentally demonstrated to increase EQE of thin film solar cells, the deep understanding of this physical mechanism hasn't been done yet.

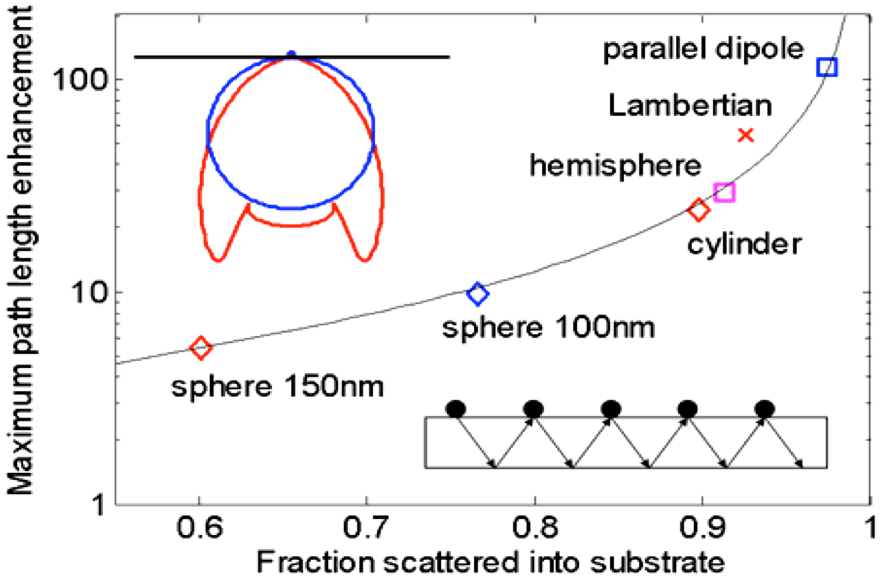

Fig. 26 Maximum path length enhancement from different metallic nanoparticles in different shape and size.[2]

More of this technique, it's found that the size and shape of the metal nanoparticles can affect the coupling efficiency.[104 105] The smaller particles have dipole moment which are closer to the photoactive layer, such help couple more light into underlying photoactive layer with improved near filed coupling. The detailed enhancement comparing of optical path length is shown in **Fig. 26**.

The coupling enhancement happens most at the peak of plasmon resonance spectrum. The spectrum can be tuned by modifying the dielectric constant of the surrounding matrix. In order to reduce the surface recombination at the metal-dielectric interface, a dielectric spacer layer can be added between metallic nanoparticles and photoactive layer. One thing needs to look out here is the fano resonance effect for frequencies above the plasmon resonance. This fano resonance effect can lead to destructive interference between unscattered and scatter light rays, which means reflection will be resulted instead of coupling.[106, 107] To solve this issue, the metallic nanoparticles can be placed at the rear of the thin film solar cells.[106] With this geometry, the light with shorter wavelength like green and blue light is absorbed in the cell before travelling to the rear contact. Near infrared light, which was poorly absorbed, will be scattered by the particles at the rear of cells and be absorbed at the later traveling. Other metallic nanostructure like metallic strips can replace nanoparticles and help trapping light. However, in order to have a improved cell with satisfied performance, other factors need to be considered, like grating diffraction effects,[108] ohmic damping, and coupling among nanoparticles and waveguide modes.[109]

2.2.8.2 Light Concentration Using Particle Plasmons

Another usage of the resonant plasmon excitation is to enhance the light absorption in the photoactive layer surrounding the metallic nanoparticles by utilizing the strong local field enhancement. This effect was used to store the energy of incident light in a localized surface plasmon mode. It works better for particles with smaller dimension (like 5-20 nm), where the albedo is fairly small.

This theory has been demonstrated in several works to show the increased photocurrent from the plasmonic near-field coupling. Organic solar cells doped with Ag nanoparticles (5nm diameter) have been showed to have enhanced performance.[110] Ag that was electrodeposited also helped organic solar cell increase the performance by the high electromagnetic field strength in the vicinity of the excited surface plasmon.[111] Other works of incorporating Ag nanoparticles also observed 1.7 times enhancement in P3HT:PCBM bulk heterojunction solar cells.[11]

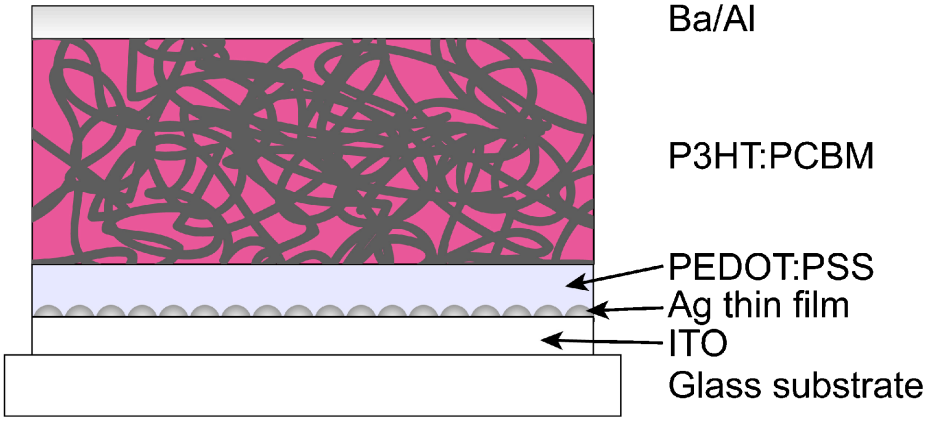

Fig. 27 Cross section of P3HT:PCBM bulk heterojunction solar cell with Ag thin film incorporated.[11]

Ag nanocavity array in an organic solar cell showed enhanced optical energy and absorption. There's a 3.2 fold improvement in PCE.[112]

2.2.8.3 Light Trapping Using SPPs

The third technique is to convert light near the interface between photoactive layer and metal back contact to form SPPs, which are electromagnetic waves. The evanescent electromagnetic SPP fields are limited around the dielectric-metal interface when close to the plasmon resonance frequency if the dimensions are smaller than the wavelength. The SPPs generated at the dielectric-metal interface can help trapping light and guide light in the

photoactive layer. With this effect, the incident light flux was rotated by 90^{o} to travel along the lateral direction inside the cell. This rotation of direction helps light absorbed more since the lateral dimension is much larger than the light optical absorption length. Since the metal contact layer is normal in most of organic solar cells as electrode layer, this kind of effect is common and should be utilized well. However, relatively high losses exist in SPPs at frequencies around the plasmon resonance frequency (usually around the visible light range). There's another factor needs to consider while using SPP. The light of SPP can also be absorbed in the metal. So the SPP trapping effect can only be effective if the light absorption of the SPP in the photoactive layer is stronger than that in the metal.

A light coupling structure needs to be incorporated in the metal-dielectric interface due to momentum mismatch between the in-plane SPPs and incident light. The coupling structure could convert the light into both SPP mode and photonic mode. The strength of both modes can be tuned by the height of the photonic structure.[113]

Several works have reported using SPPs in organic solar cells. In a Ag/CuPC/C_{60}/BCP/Ag structured solar cell, it's shown that the EQE at wavelength of 532 nm is doubled at resonance to 12%.[114] The improvement is due to enhancement in the absorption from the conversion of incoming light to guided SPPs. The nonradiative losses and SPP scattering are pretty trivial. However, the device did suffer from the loss of SPP and photonic excitation due to metal penetration into photoactive layer.

Another similar work on CuPC/C_{60}/BCP based organic solar cell also studied the SPPs effect the performance of device.[5] There is a boost in the absorption gap between the phthalocyanine Q and Soret bands as seen in **Fig. 29**. A special light absorbing "antenna" layer in inserted outside of the photoactive layer as illustrated in **Fig. 29**. The light absorption

would be decoupled from the exciton diffusion then. The light absorbed by this antenna layer would be transferred to the photoactive layer by the surface plasmon polaritons at the interface of photoactive layer-metal layer(which is a thin silver layer inserted). The measured peak efficiency of energy transfer can be around 51%.

The usage of photonic structure at the dielectric-metal interface was demonstrated in a organic bulk heterojunction solar cell, with photoactive materials of polyfluorenes and fullerene derivative.[16] SPPs are triggered at the dielectric-metal interface and help increase light absorption and photocurrent. It's found there is larger enhancement in the photocurrent at the plasmon resonance peak.

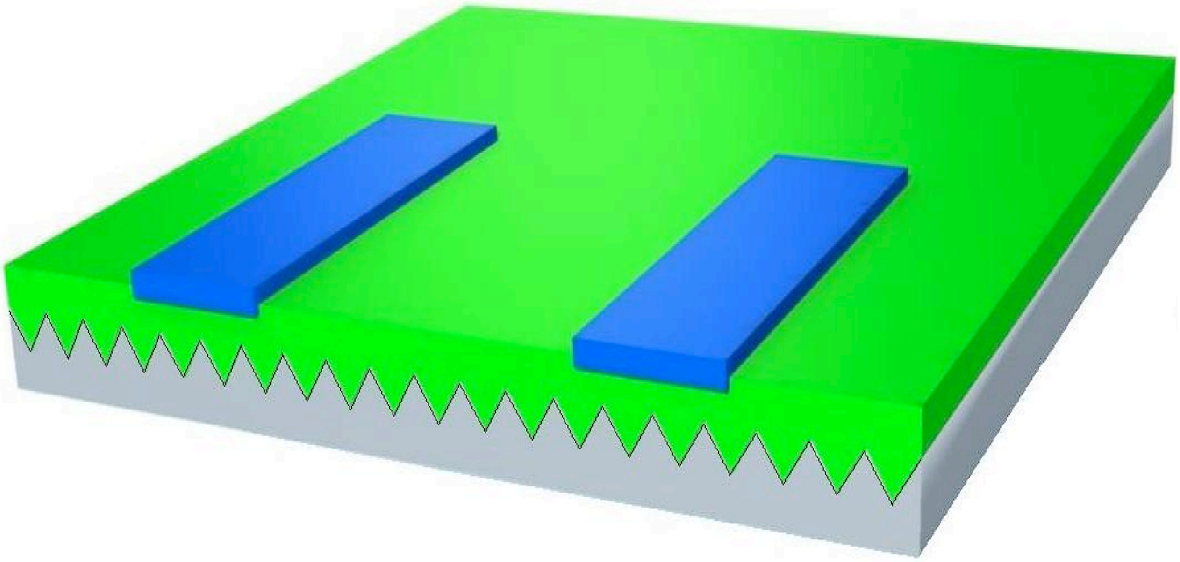

Fig. 28 Schematic drawing of the inverted solar cell with nanostructured bottom cathode and transparent PEDOT:PSS anode.[16]

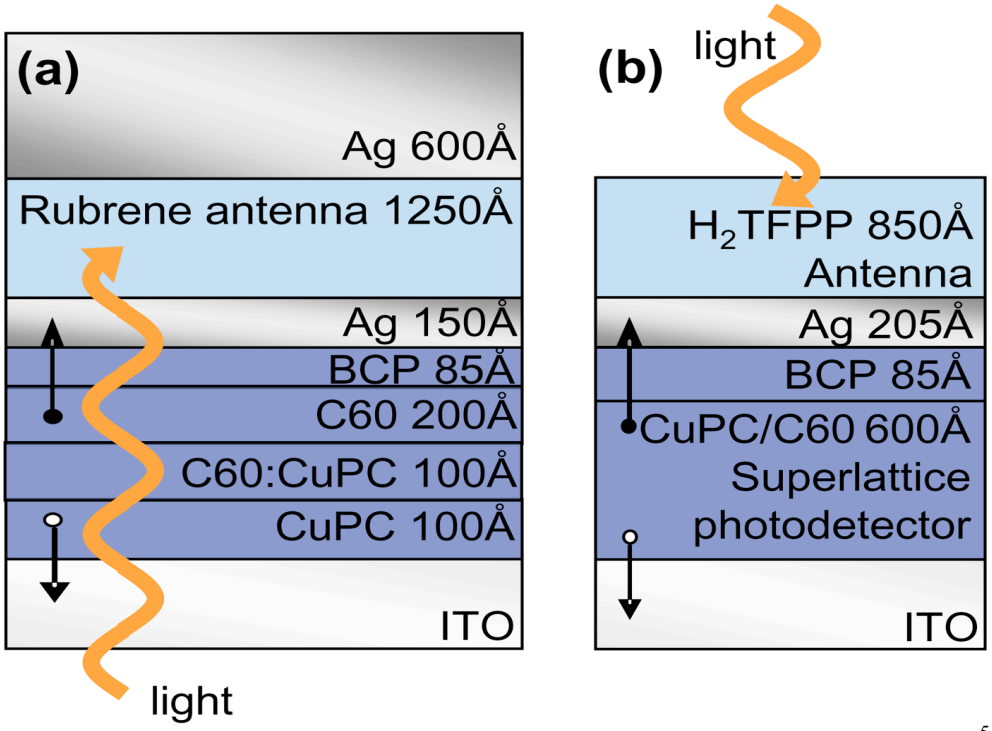

Fig. 29 Schematic diagram of OPV devices with intermediate antenna layer.[5]

All in all, non-planar metal back reflector based solar cells can have combined effects of geometric scattering, higher local fields and scattering into photonic and plasmonic modes. There are quite some works of using textured metal back reflector on organic solar cells to trap light. [16, 115]

Another interesting work to trap light is using dual photonic crystals by combing the surface coupler with SPPs.[116] In this work, there is a layer of polymer microlens with period of 500 nm on the glass. It can help focus incident light from this periodic structure and have strong diffracting effect inside the active layer. The back metal has a photonic-plasmonic crystal. At the dielectric-metal interface, it can both generate surface plasmon modes and waveguiding modes to enhance longer wavelength absorption. There has seen enhancement of 49% in light absorption and enhancement of 58% in photocurrent compared to flat cell in nearly lossless metal contact.

CHAPTER 3.

MICROLENS ARRAY INDUCED LIGHT ABSORPTION ENHANCEMENT IN OPV DEVICES

3.1 Abstract

Over the last decade, organic photovoltaic devices have attracted a lot of attention and highest power conversion efficiencies are now close to 10%. Here we employ an optical structure - microlens array - to increase light absorption inside the active layer, and PCE of OPVs increased even for optimized devices. Normal incident light rays are refracted at the MLA and travel longer optical paths inside the active layers. Two OPVs systems - poly(3-hexylthiophene-2,5-diyl):(6,6)-phenyl C61 butyric acid methyl ester (P3HT:PCBM), and poly[[9-(1-octylnonyl)-9H-carbazole-2,7-diyl]-2,5-thiophenediyl-2,1,3-benzothiadiazole-4,7-diyl-2,5-thiophenediyl]:(6,6)-phenyl C71 butyric acid methyl ester (PCDTBT:$PC_{71}BM$) - were investigated. In the P3HT:PCBM system, MLA increased the absorption, absolute external quantum efficiency , and the PCE of an optimized device by ~ 4.3%. In the PCDTBT:$PC_{71}BM$ system, MLA increased the absorption, absolute external quantum efficiency, and PCE by more than 10%. In addition, simulations incorporating optical parameters of all structural layers were performed and they support the enhancement of absorption in the active layer with the assistance of MLA. Our results show that utilizing MLA is an effective strategy to further increase light absorption in OPVs, in which optical losses account for ~40% of total losses. MLA also does not pose materials processing challenges to the active layers since it's on the other side of the transparent substrate.

3.2 Introduction

In this era of depleting fossil fuel based energy sources, and their environmental impact, focus on renewable energy sources is becoming increasingly important. Direct conversation of solar energy to electricity is very attractive due to the abundance of solar energy resource, which dwarfs all other energy resources combined. Within the solar cell community, polymer-based solar cells (OPVs) have received heightened attention due to advantages such as flexibility, potentially low cost production, lightweight and easy integrability into building products, clothes and fabrics. OPVs have been making rapid progress in research and development in academia and industry; maximum power conversion efficiencies (PCE) have increased from around 2% to 10% in the last decade[32, 33]. This progress is owing to the development of new materials, and novel device structures and processing conditions. So far, majority of studies on OPVs have focused on the development of new materials,[34-36] interlayers,[7, 37, 38] and morphology optimization.[39-43] Another important way to enhance the PCE of OPVs is by increasing light absorption inside the active layers using various optical approaches. Enhancing light absorption is important because active layers in OPVs are quite thin, which leads optical losses accounting for ~40% of total losses.[117] In true bilayer donor-acceptor heterostructures, active-layers can only be ~10 nm thick due to short exciton diffusion lengths (around 5~10 nm[118]). On the other hand, in bulk-heterojunction structures, in which the donors and acceptors are intimately mixed together in a single layer, higher thickness can be afforded. However, such thicknesses (~ 100 – 200 nm, at times less) are still not enough to efficiently absorb light, and thicknesses cannot be indiscriminately increased further because of low charge carrier mobilities in most organic

materials. Hence, to boost efficiencies further, it is imperative to improve light absorption within existing OPV architectures.

Some optical approaches enabling light trapping in OPVs have been proposed and implemented. These include approaches like textured substrates,[12] wrinkles and deep folds,[85] metal nanospheres,[119, 120] and microlens arrays.[121] However, these methods suffer from one or more weaknesses. In case of textured substrates, topographical dimensions of textures (gratings) need to be designed optimally to enable a conformal coating of active layers. High aspect-ratio gratings can result into shunts between top and bottom electrodes, underfilling, and air gaps inside active layer film.[12] Whereas, narrow pitch gratings lead to overfilling of trenches and increased losses from carrier recombination.[12] Another challenge is that for different polymer systems with different optimum active-layer thicknesses, grating dimensions need to be redesigned and retested for conformal polymer coating. The approach of utilizing substrates with wrinkles and deep fold features suffers from similar issues. Besides, it is challenging to have a quantitative and precise control on the dimensions of self-assembled wrinkles and folds. Utilizing metal nanospheres inside active layers employs plasmonic near-field enhancement effects to trap more light. However, this approach also has drawbacks such as inclusion of metallic and surface group impurities, which could act as recombination centers and degrade charge transport. Utilizing microlens array (MLA), as an additional structure on the side of the transparent substrate opposite to the active-layer, is another approach to increase light absorption inside the active layer of OPVs. Since MLA is located on the other side of the substrate, this approach is non-intrusive in nature, and has no effect on the device fabrication processing or internal morphology of the active-layer. It has also been demonstrated as a universal method of light absorption enhancement in different

organic photovoltaic systems.[121] In this previous demonstration, MLA consisted of hemispherical microlenses with diameter 100 μm. These 100 μm microlenses reduce surface-reflection, and refract the incoming light towards the active layer, thus increasing the optical path. In this study, we utilized the near-hemispherical microlenses of 2μm diameter. With a sharper peak the near-hemispherical shape is better in getting light beams larger refraction angles. These microlenses, with diameter close to visible light wavelength, not only reduce surface reflection and refract incoming light like 100 μm microlens, but also utilize optical interference to enhance light intensity inside active layer. Even though 100 μm MLAs are acting as gratings, the diffractive angles are very small, which makes the diffraction very small and hard to observe. However, 2 μm MLAs have period closer to visible light wavelength, which makes the diffractive angles larger than that of 100 μm MLAs. The more diffractive nature of 2 μm period compared to 100 μm period makes the light enhancement in 2 μm MLAs higher. This is indicated by simulations on MLAs with diameter 2 μm and diameter 6 μm. Since 6 μm is much larger than visible light wavelength (short wavelength limit), light absorption in the OPVs can be studied with geometrical optics, or ray optics, where optical effects such as diffraction and interference are not accounted for (the diffraction effect is very small as discussed above). In this short wavelength limit, the 6 μm and 100 μm MLAs yield the same light absorption enhancement. We show these simulation results in the simulation section of this paper. We fabricated two types of OPVs on our MLA substrates and compared their performance with devices without MLA. Performance enhancement in MLA devices is demonstrated in the following sections through different characterizations and discussion.

3.3 Methods and Experimental

3.3.1 Microlens Array

The MLA is composed of arrays of microlenses as shown in **Fig. 30**. Microlenses were near-hemispherical with a diameter of 2μm, and they sit on the side of glass substrate facing the incident light. The array is fabricated by imprinting a polydimethylsiloxane (PDMS) mold on a UV curable polyurethane (PU) drop placed on the glass. More details about fabrication of MLA on glass are described elsewhere.[122]

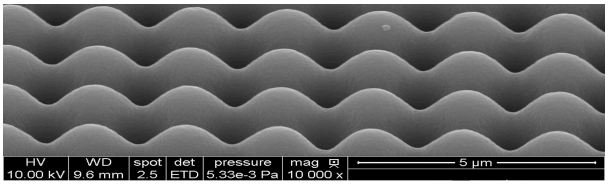

Fig. 30 SEM image of PU layer with MLA pattern

3.3.2 P3HT:PCBM OPV System

P3HT (Solarmer Inc.) and PCBM (Nano-C Inc.) were dissolved in 1,2-dichlorobenzene (o-DCB) with 20mg/ml concentration for each and stirred at 800 rpm on a hot plate with temperature of 45^{o}C for around 20 hours to make active layer solution. Indium Tin Oxide (ITO) coated glass (Delta Technologies) and ITO coated glass with MLA pattern were ultrasonicated in 2-propanol/acetone, and de-ionized water, respectively for 2 minutes. Then both substrates were dried with nitrogen and exposed to air plasma 1 minute. Poly (3, 4-ethylenedioxythiophene):Poly (styrenesulfonate) (PEDOT:PSS) was spin-coated on the ITO side of the glasses at 3000 rpm for 60s. Spin-coated devices were annealed on a hot plate at 100^{o}C for 10 minutes. Both substrates were then transferred inside a glovebox filled with nitrogen. The previously prepared active layer solution was filtered through a 0.2 μm filter. Filtered solution was dropped on the PEDOT:PSS film devices and spun at the speed of 500

rpm for 45 seconds. After spin-coating, devices were covered under separate petri dishes for 1 hour. This amount of time is long enough to dry the active layer and its color changes from orange to dark purple. Devices were then taken out from petri dishes and annealed on a hot plate at 110^{o}C for 10 minutes. After annealing, devices were transferred to a thermal evaporator with loaded calcium (Ca) and aluminum (Al) source. Under a vacuum level of around 10^{-6} mbar, 25 nm of Ca was evaporated on the active layer, followed by 100 nm of Al layer. Under the same fabrication process, there were six cells made with top electrode contact area of 0.1256cm^2 in one batch. In total, there were two batches made, where the second batch was made with the same fabrication process, except from lower active layer solution concentration of 10mg/ml.

3.3.3 PCDTBT:$PC_{71}BM$ OPV System

PCDTBT of molecular weight 50kD was purchased from 1-material. M_OO_X (99.99%), LiF (99.98%) and $PC_{71}BM$ were purchased from Sigma Aldrich. For the PCDTBT:$PC_{71}BM$ system, 10 nm of M_OO_X anode buffer layer was thermally evaporated on ITO under a vacuum of about 10^{-6} mbar with rate 0.5 Å/sec. A solution of PCDTBT and $PC_{71}BM$ (volume ratio 1:3.5), with a concentration of 7 mg/mL in dichlorobenzene (DCB) was kept stirring on a hot plate at 90^{o}C and 650 rpm for eight hours. After that, the temperature of the solution was reduced to 600^{o}C at the same stirring speed. After several days, the active layer was spin coated on the top of M_OO_X layer at 2000 rpm for 45 seconds. The devices were dried under petri dish for 20 min, and then annealed for 15 min on a hot plate at 700^{o}C. Finally, LiF (2nm) and Al (130 nm) were thermally evaporated over the active layer with a shadow mask of area 0.1256 cm^2 with evaporation rate less than 0.5 and 8

Å/sec, respectively. Under the same fabrication process, there were six cells made in one batch. In total, there were three batches made.

3.3.4 Characterization

Several characterizations were carried out as described below. Current-Voltage characterization was done using ELH Quartzline halogen lamp at 1 sun intensity, which was calibrated using a reference crystalline Si solar cell coupled with a KG-5 filter. Absolute external quantum efficiency (EQE) was done using a custom setup built from a single grating monochromator (Horiba Jobin Yvon Srl), 100W halogoen bulb (OSRAM Bellaphot), and a current preamplifier (Ithaco, Inc.). An optical chopper (Thor Labs) coupled with a lock-in amplifier (Stanford Research Systems) were also used to reduce noise in the system. EQE was carried out at room temperature with ambient light present. For absorption characterization, ITO coated glasses were deposited with PEDOT:PSS (for P3HT system) or M_OO_X (PCDTBT system) and active layer following the fabrication process in the previous sections. Then these active-layer coated substrates were optically characterized with a Varian Cary 5000 UV-Vis-NIR spectrophotometer. Global reflection and global transmission were obtained from the spectrophotometer. Then absorption was calculated using 100% subtracting global reflection and global transmission.

3.4 Results and Discussion

We chose to investigate P3HT:PCBM system because it is the most widely investigated system in the field of OPVs. Even though new promising materials have

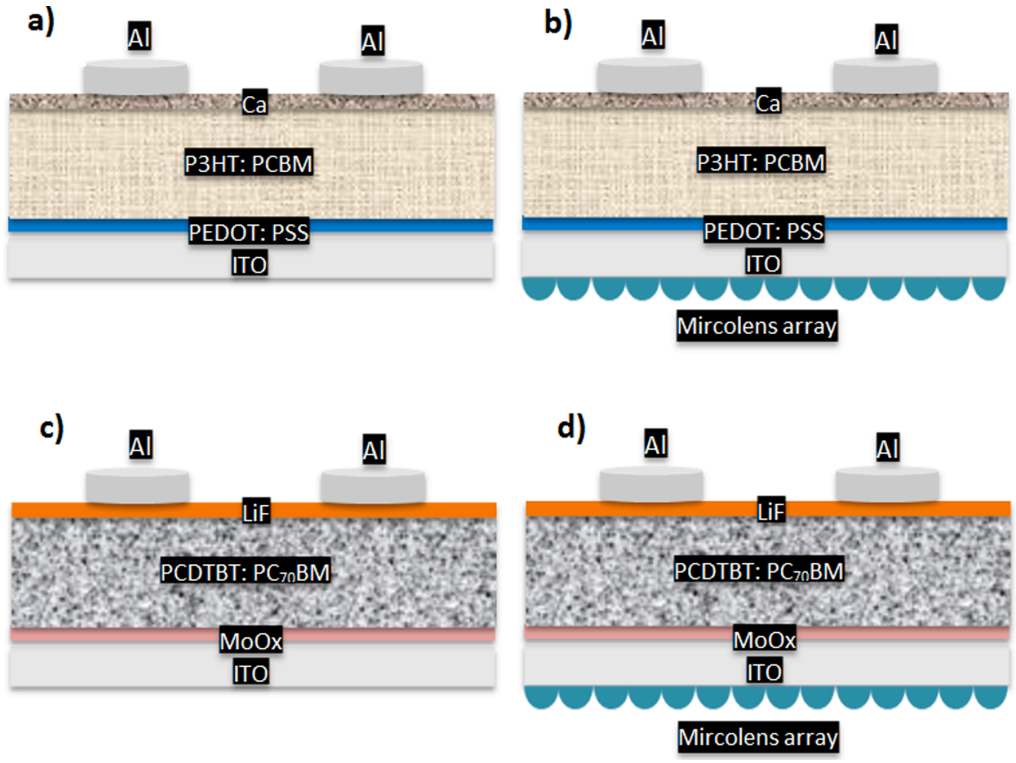

Fig. 31 Schematic structures of different OPV systems: P3HT:PCBM system (a) without MLA and (b) with MLA; PCDTBT:$PC_{71}BM$ system (c) without MLA and (d) with MLA

emerged recently, P3HT:PCBM systems remains relevant for one of the sub-cells in tandem structures. Illustrated in **Fig. 31(a)** is a conventional P3HT:PCBM device, which is our control device in this study. Corresponding P3HT:PCBM device with an additional layer of

Table 1 Parameters of current-voltage characterization of two OPV systems with and without 2μm MLA.

System	**P3HT:PCBM**		**PCDTBT:$PC_{71}BM$**	
Parameters	**J_{sc} (mA/cm^2)**	**PCE (%)**	**J_{sc} (mA/cm^2)**	**PCE (%)**
Control	11.78	4.69	12.75	5.6
MLA	12.29	4.89	14.12	6.4
Enhancement	4.3%	4.3%	10.7%	14.3%

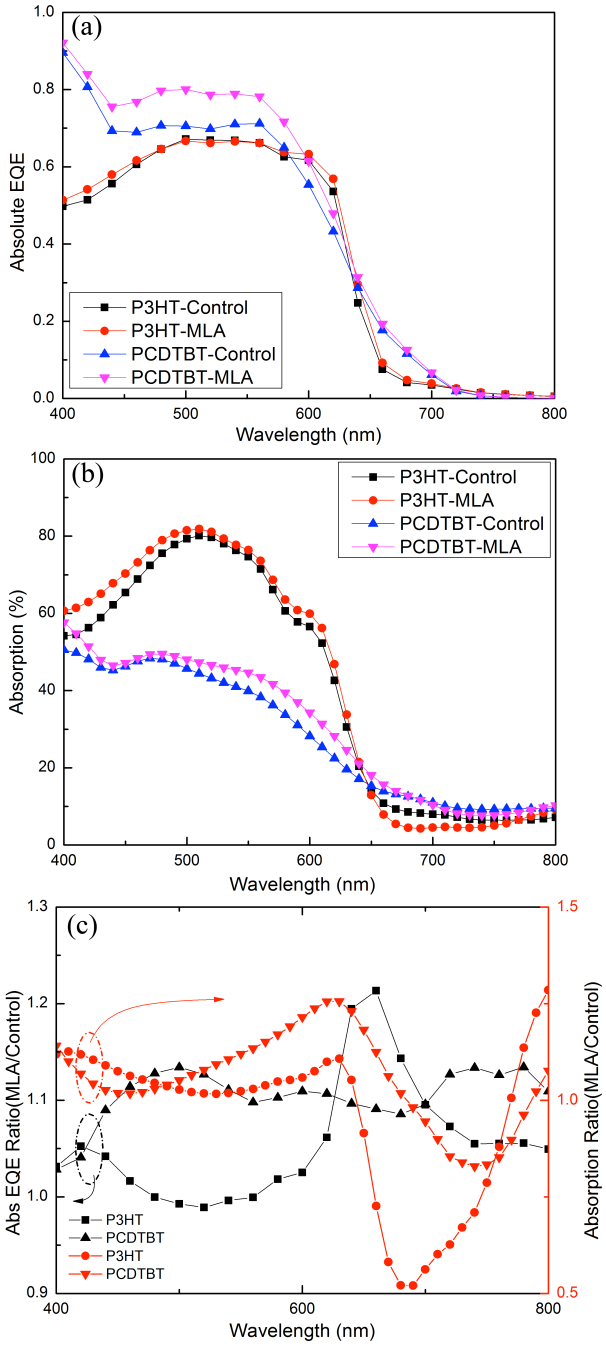

Fig. 32 (a) Absolute EQE of P3HT:PCBM and PCDTBT: $PC_{71}BM$ devices without (control) and with (MLA) MLA. (b) Absorption of P3HT:PCBM and PCDTBT: $PC_{71}BM$ devices without (control) and with (MLA) MLA. (c) Abs EQE ratio of MLA device to control device (black color); Absorption ratio of MLA device to control device (red color).

MLA on one side of glass (called MLA device) is schematically shown in **Fig. 31(b)**. The performance parameters of current-voltage characterization of the two devices are listed in table 1. The performance parameters of each device in the table are averaged from six cells in one batch. Since the devices were fabricated with optimized conditions from our experience and through literature, It can be observed that even control device has a quite high PCE around 4.69%, one of the highest among P3HT:PCBM devices in literature. The performance of MLA device increases by 4.3% to 4.89%. This improvement is due to enhancement of current density (J_{sc}), which increases from 11.78 mA/cm^2 in control device to 12.19 mA/cm^2 in MLA device. The performance enhancement in percentage is not as high in our case as in the previous

P3HT:PCBM study with 100 µm microlenses. However, it should be noted that our fabrication conditions are more optimized, and even our control P3HT:PCBM device performs better than the MLA P3HT:PCBM device in that study.

In **Fig. 32(a)**, MLA device shows higher absolute EQE than control device in the wavelength between 400 nm to 800 nm. From a quantitative view of this enhancement as in **Fig. 32(c)**, the enhancement from MLA reaches up to 5% in the shorter wavelength range below 600 nm, while in the wavelength range above 600nm the enhancement can be as high as 20%. Since MLA layer is on the separate side of glass substrate from device structure, the microlenses do not affect the process of exciton diffusion/dissociation, charge transport and collection. However, the MLA layer can change the direction and distribution of incoming light in the active layer. Incoming light beams get refracted through MLA and have longer optical paths compared to those without MLA. Longer paths give light more chance to be absorbed inside active layer. Besides, light beams, which get reflected on one microlens would encounter another neighboring microlens and get refracted into the active layer, thus reducing surface reflection. At the same time, close-packed MLA with diameter 2µm close to visible light wavelength acts as structured gratings to produce diffraction pattern inside active layer. This diffraction would enhance light intensity inside active layer, contributing to more exciton creation and hence charge carriers. The light absorption spectra inside active layer of P3HT:PCBM devices are measured and depicted in **Fig. 32(b)**. As shown in **Fig. 32(c)**, between wavelengths 400 nm and 650 nm, MLA leads to broadband enhancement of light absorption inside the active layer, with the highest enhancement up to 10%. In wavelength range between 650nm and 780nm, there is reduction in light absorption in MLA device compared to the control device. It may be caused by light interference in this wavelength

region, which reduces light intensity inside active layer. However the light absorption in this range is far smaller than that below 650nm. This little reduction of light absorption does not significantly change the total light absorption enhancement. Thus, it can be seen that by simply adding a MLA layer on glass substrate, P3HT:PCBM device gets more light absorption in the active-layer, leading to more higher current density and higher PCE.

In PCDTBT:$PC_{71}BM$ devices, with similar structure and same function of MLA in OPV devices, we expected that the light absorption, absolute EQE and the current density will also increase. In fact, we expected higher enhancement because PCDTBT:$PC_{71}BM$ active layers are only 70 nm thick in optimized devices.[123] In order to verify our hypothesis, the similar characterization of PCDTBT:$PC_{71}BM$ system as the P3HT:PCBM system was carried out. From table 1 it is clear that the short circuit current density is enhanced by 10.7%, and PCE is increased from 5.6% to 6.4%. The spectra of the absolute EQE in Fig. 3(a) also clearly show an enhancement in case of MLA device, supporting the current density enhancement. In the wavelength region between 450 nm to 800 nm, the enhancement of EQE is slightly larger than 10% as seen in **Fig. 32(c)**. The light absorption spectra, shown in **Fig. 32(b)** also support our expectation about the effect of the MLA. The light absorption inside the active layer is enhanced from MLA in the entire region between 400 nm and 700 nm, except a little reduction between 700 nm and 800 nm. As seen in **Fig. 32(c)**, between 400 nm and 550 nm, the enhancement falls below 10%. The enhancement between 550 nm and 650 nm becomes higher than 10% and reaches a maximum of 26% at 625nm.

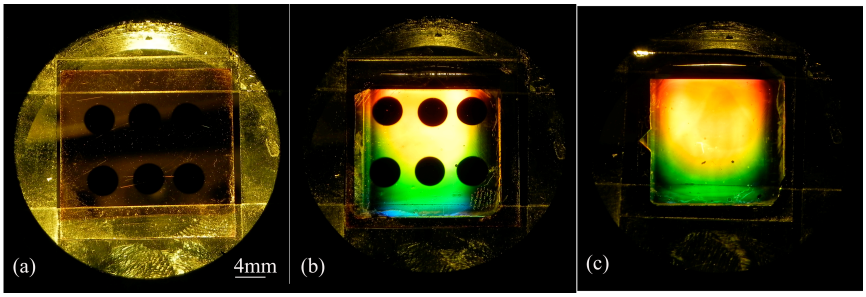

Fig. 33 Optical photos taken above devices with light of Halogen lamp shining through devices from bottom. (a) Control device without MLA, (b) MLA device with MLA, (c) ITO coated glass with MLA

The existence of diffraction effect from MLA is demonstrated in **Fig. 33**. The measurement was carried out on a ground. On the ground there is a big hole, which is larger than OPV devices. One halogen lamp was put just under the hole at some distance so that light can shine through the hole. Three devices with P3HT:PCBM active layer: control device, MLA device, and ITO coated glass with MLA were put above the hole in turn experiencing the same light condition. Then optical photos were taken above the devices using a digital camera with the same setup. Control device, which has no MLA layer, shows conformal light mapping as seen in **Fig. 33(a)**. However, **Fig. 33(b)** and **Fig. 33(c)** show diffraction pattern in device with MLA and glass with MLA, respectively. Microlenses are behaving like small diffraction gratings in the micrometer scale, which generate colourful mapping from the visible light. Thus the combination of hundreds of small diffraction gratings obviously forms diffraction and interference patterns inside the active layer as well, thus further increasing effective optical path. The enhanced light intensity contributes to more exciton creation and charge carriers inside the active layer. The above colourful mappings on the surface are for substrates with 2 μm MLA, obviously showing the diffraction effect. However substrate with 100 μm MLA didn't show the colourful mapping on device surface (not shown here in this paper). Even though 100 μm MLA is a periodical

grating structure, the diffractive angle is very small since the period is far larger than visible wavelength. So there's barely diffraction effect observed in 100 μm MLA devices. With MLA grating period reduced to 2 μm, the diffractive angle increases and shows diffraction effect as seen in the colourful mapping. So 2 μm MLA would enhance more light absorption than 100 μm MLA.

In summary, MLA brings enhancement in these two OPV systems. Because the thickness of active layer in P3HT:PCBM (around 200 nm) is far larger than that in PCDTBT: $PC_{71}BM$ (around 70 nm) , the light absorption in the first system is already high enough while the light absorption in the second system is lower. So the light absorption enhancement effect of MLA in the second system is more prominent than that in the first system. This indicates that MLA is an effective way to enhance light absorption in OPV systems, especially when light absorption in the original device is not very high.

3.5 Simulation

Light absorption simulation is done for both OPV systems with both control and MLA devices as shown in **Fig. 34(a)**. The simulation of these devices is based on the structures in **Fig. 31**. Planewave-based transfer matrix method[124-126] is applied as a full-field electromagnetic approach to obtain the absorption spectrum. In the simulation, the wavelength range is restricted to 400 nm to 800 nm to match the solar spectrum and the two OPV systems' absorption. Optical parameters of refractive indices n and the extinction coefficients k are obtained from the literature.[59, 127-129] **Fig. 34(a)** shows the simulated absorption for both OPV systems with control and MLA devices, revealing the higher absorption in MLA devices than that in control devices. In the wavelength range between

400nm and 650nm, where most of light was absorbed for P3HT devices, the light absorption in MLA device shows enhancement as large as 10% around 400nm and 570nm, with average of improvement around 4% compared to control device. The simulated light absorption of PCDTBT devices expe70riences average of 9% enhancement in MLA device than control device between light wavelength of 400nm and 650nm. In order to confirm our expectation of higher light absorption with 2 µm MLA than that with 100 µm MLA, simulation with both 2 µm MLA and 6 µm MLA is employed and shown in **Fig. 34(b)**. MLA with diameter 6 µm is far larger than visible light wavelength, which only plays a ray optic effect to increase light optical path inside active layer, similar to MLA with diameter 100um. Below 600 nm, the absorption spectra show an average of 4% higher absorption in 2 µm MLA than in case of 6 µm MLA, where most of light absorption happens. From these simulations, we can more confidently say that employing 2 µm microlens arrays is a more effective way to enhance the performance of OPVs, than MLAs with much greater dimensions. Of course, 2 µm might not

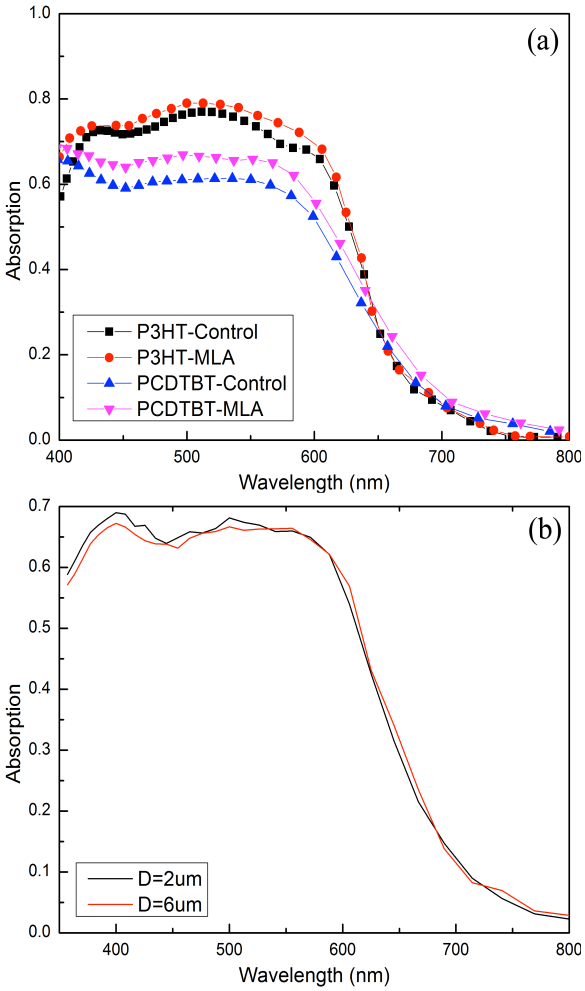

Fig. 34 (a) Simulation of light absorption inside active layers of P3HT:PCBM and PCDTBT:$PC_{71}BM$ devices for without (control) and with (MLA) MLA. (b) Absorption simulation spectra of PCDTBT:$PC_{71}BM$ devices with MLA of diameter 2µm and 6µm.

be the most optimal dimension and in the vicinity of these dimensions, there might be once that can perform better. That exploration is a part of our current and future studies.

3.6 Conclusion

In this work, two types of OPV systems: P3HT:PCBM, PCDTBT:$PC_{71}BM$ are investigated with 2μm microlens array on one side of glass substrate. Devices with MLA have a better performance than that without MLA. In P3HT:PCBM system, MLA increases the absorption, absolute external quantum efficiency, and PCE by 4.3%, even for a conventional device with fabrication conditions optimized for high efficiency. In PCDTBT:$PC_{71}BM$ system, MLA increases the absorption, EQE and PCE by more than 10%. All of these enhancements are due to increased light path and absorption inside active layer from refracted light through microlens as well as diffraction induced light intensity enhancement. This improvement of light absorption is further supported by simulations in the two OPV systems. Our MLA approach is more effective in devices with thinner active layer than that with thicker active layer. MLAs also do not pose materials processing challenges to the active-layers since they are on the other side of the transparent substrate.

CHAPTER 4.

INVESTIGATION OF DEPENDENCE OF MICROLENS DIMENSIONS ON LIGHT-ABSORPTION ENHANCEMENT IN OPV DEVICES

4.1 Abstract

The performance of organic photovoltaic devices is improving steadily and efficiencies have now exceeded 10%. However, incident solar spectrum still largely remains poorly absorbed. To reduce optical losses, we employed a microlens array (MLA) layer on the side of the glass substrate facing the incident light; this approach does not interfere with the processing of the active-layer. We observed up to 10% enhancement in the short circuit current of poly((4,8-bis[(2-ethylhexyl)oxy]benzo[1,2-b:4,5-b′]dithiophene-2,6-diyl)(3-fluoro-2-[(2-ethylhexyl)carbonyl] thieno[3,4-b]thiophenediyl)):(6,6)-phenyl C71-butyric acid methyl ester (PTB7:$PC_{71}BM$) OPV cells. Theoretically and experimentally investigating several MLA dimensions, we found that photocurrent increases with the ratio of height to pitch size of MLA. Simulations reveal the enhancement mechanisms: MLA focuses light, and also increases the light path within the active-layer by diffraction. Photocurrent enhancements increase for thinner active- layers, as demonstrated in poly[N-9′-heptadecanyl-2,7-carbazole-alt-5,5-(4′,7′-di-2-thienyl-2′,1′,3′-benzothiadiazole)] (PCDTBT):$PC_{71}BM$ OPV devices with 17% improvement in short circuit current.

4.2 Introduction

Solar-electric conversion using organic semiconductors has been a very active research area within the photovoltaic community. OPV devices have the advantages of

flexibility, light weight, and potentially low cost roll-to-roll production.[130] In the last decade, power conversion efficiency (PCE) of OPV devices has increased from 2% to 11%.[32, 33] The rapid improvement of PCE has primarily been due to the following aspects: (1) new materials, especially small band-gap donor polymers with appropriate energy level offsets to the fullerene acceptors,[34-36] (2) improved anodic and cathodic buffer layers,[7, 37, 38] and (3) the optimization of the bulk-heterojunction morphology using approaches such as annealing and additives.[39-43] Although the OPV efficiencies have improved steadily, they still are lower than those of contemporary thin-film inorganic solar cells. The efficiency losses in OPV cells include thermalization, exciton recombination, energy losses required for exciton dissociation, charge-carrier recombination, and optical losses. Among them, optical losses have been estimated to be nearly 40% of total losses.[117] This is primarily because the thicknesses of OPV active-layers, as optimized for efficient charge transport, are only 100-200 nm or less. Therefore, methodologies to improve light absorption are necessary for further advancement of OPV technology.

In addition to tailoring the band-gap of materials to absorb more solar spectrum, several device architectural approaches have been explored to improve light absorption in OPV devices. These include utilizing textured substrates,[8, 12, 131] substrates with wrinkles and deep folds,[85] metal nanoparticles in or adjacent to the active-layers[119, 120] and patterning the active-layers.[132] However, these approaches bring along several challenges and bottlenecks. In the textured substrate approach of Nalwa et al., texture dimensions need to be tailored, or rather discovered by trial-and-error for conformal coating of active-layers. Low-aspect ratio structures lead to over-filling of trenches and increased charge-carrier recombination, and high-aspect ratio structures lead to catastrophic shunts between the electrodes. Additionally,

for contemporary polymer systems, which typically have thinner active-layers, achieving conformal coatings will be more challenging. Overall, conformally patterned cells may have good theoretical performance for optimum optical designs, but realizing conformal coatings by solution-processing is non-trivial and an open problem. The microprism approach, and the one of utilizing substrates with wrinkles and deep folds suffer from similar issues. In the latter, it is also challenging to have a quantitative and precise control on the dimensions of self-assembled wrinkles and folds. Incorporating metal nanoparticles in or adjacent to the active-layer can also improve light absorption by surface plasmon polarization assisted field enhancement, and lateral propagation of light in the plasmonic mode.[11, 111, 119, 120, 133] However, metal nanoparticles are centers for exciton quenching and charge-carrier recombination. In summary, all of the above approaches are intrusive to the active-layer, and optical enhancement often comes at a cost of disrupting the charge dynamics.

An alternative non-intrusive approach is employing microlens array (MLA) on the side of the transparent substrate opposite to the active-layer, such that light traverses the MLA and transparent substrate before entering the active-layer. Being on the other side, MLAs do not affect the fabrication or morphology of the active-layer. The MLA approach has been successfully used in organic light-emitting diodes to enhance light extraction.[134-137] More recently, MLA approach was also demonstrated to be useful for OPV devices. Myers et al. utilized hemispherical microlenses with 100μm diameter;[121] this led to refraction of light towards the active-layer and reduced surface reflection. In our previous publication,[138] we showed that MLA with smaller features sizes can be more promising because besides reduced surface reflection and refraction, they can also benefit from diffraction. In that report, we only investigated 2μm diameter microlenses, but by smaller feature sizes we more

generally mean feature sizes in or near the regime of optical wavelengths. Feature sizes (diameters) smaller than 2μm have not been explored; neither has been the effect of changing the height of microlenses. That is the focus of this report, in which we show that both the pitch and height of microlens structures critically affect the device performance. We couple experimental investigations with theoretical predictions, for two contemporary polymer systems (PTB7 and PCDTBT). Simulations also elucidate the mechanisms behind enhancement in light-absorption.

4.3 Experimental Section

4.3.1 Microlens Array Fabrication

Periodic MLA with square lattice symmetry, having a structure similar to a closely packed egg tray, was fabricated by soft lithography imprinting on polyurethane from a polydimethylsiloxane (PDMS) mold. Polyurethane was then cured under UV light for 3 hours, forming a solid MLA pattern after peeling off the PDMS mold. MLAs with different pitches were fabricated from PDMS molds of different pitches. The PDMS molds with varying pitches and the desired inverse relief patterns were obtained from holographic interference lithography of photoresist. Further details about fabrication of MLA pattern and PDMS molds are described elsewhere.[122] The fabricated MLA with different pitch sizes can be seen in **Fig. 35**.

4.3.2 Device Fabrication

PTB7 (1-Material) and $PC_{71}BM$ (1-Material) with a weight ratio 1:1.5 were dissolved in 1,2-dichlorobenzene:1,8-diiodoctane (97%: 3% by volume) with 25 mg/ml total concentration, and stirred at 800 rpm on a hot plate at a temperature of 60^{o}C for around 20

hours. Indium Tin Oxide (ITO) coated glasses (Delta Technologies) with and without MLA pattern were pre-cleaned by sonicating in 2-propanol/acetone and then de-ionized water for 10 min each. The substrates were then dried with nitrogen and exposed to air plasma for 1 minute. Poly (3, 4-ethylenedioxythiophene):poly (styrenesulfonate) (PEDOT:PSS) was spin-coated on ITO substrates at 4000 rpm for 60 s, followed by annealing on a hot plate at 120^{o}C for 10 min. The substrates were then transferred inside a nitrogen-filled glovebox. The previously prepared active-layer solution was filtered through a 0.2 μm filter, dropped on the PEDOT:PSS coated ITO, and spin-coated at 1000 rpm for 60 seconds. After spin-coating, the devices were covered with separate petri dishes for 2 hours. This length of time was long enough to dry the active-layers. To finish the device fabrication, 20 nm calcium and 100 nm aluminium were thermally evaporated on the active-layer at a pressure of around 10^{-6} mbar. The preparation of substrates for PCDTBT based devices was done similar to that of PTB7. PCDTBT of molecular weight 50k D was purchased from 1-Material. M_OO_X (99.99%), LiF (99.98%) and $PC_{71}BM$ were purchased from Sigma Aldrich. For the PCDTBT:$PC_{71}BM$ system, 10 nm of MoO_X anodic buffer layer was thermally evaporated on ITO under a vacuum of about 10^{-6} mbar at the rate of 0.5 Å/sec. Solution of PCDTBT and $PC_{71}BM$ (volume ratio 1:3.5), with a concentration of 7 mg/mL in dichlorobenzene was continuously stirred on a hot plate at 90^{o}C and 650 rpm for 8 hours. The temperature of the solution was then reduced to 60^{0}C at the same stirring speed. The active-layer was then spin coated on the top of the MoO_X anodic layer at 2000 rpm for 45 seconds. The films were dried under petri dishes for 20 min, and then annealed for 15 min on a hot plate at 70^{0}C. Finally, LiF (2 nm) and Al (130 nm) were thermally evaporated on the active-layer at the rates of 0.5 and 8 Å/sec,

respectively. PTB7 and PCDTBT based device architectures without and with MLA are depicted in **Fig. 36**.

4.3.3 Experimental Characterization

For global transmission measurements, 0% and 100% were first calibrated for the integrating sphere. ITO coated glass substrates with and without MLA were placed in front of the opening of integrated sphere with ITO layer facing the opening. Then global transmission spectra were recorded from the optical fiber coupled spectrometer (Ocean Optics). For current density-voltage characterization, ELH Quartzline halogen lamp provided 1 sun illumination after being calibrated with a reference crystalline Si solar cell coupled with a KG-5 filter. All the samples were measured under the same light intensity. In order to measure external quantum efficiency (EQE), a 100 W halogen bulb (OSRAM Bellaphot) was used as a light source with a single grating monochromator (Horiba Jobin Yvon Srl). An optical chopper (Thor Labs) coupled with a lock-in amplifier (Standford Research Systems) was employed to reduce system noise. The EQE spectra were calculated after comparing the sample signal to the crystalline Si reference signal. Light angle dependent current density was measured using a customized setup in the lab. 1 sun illumination was obtained using a light source (LS150 Abet technology) and calibrated with a reference crystalline Si solar cell. A rotating sample stage was used to change the incident angles from 0 to 80 degrees, and short-circuit current was measured using Keithley 2400 sourcemeter.

4.3.4 Simulations

We used the rigorous scattering matrix (SM) method,[124, 139] where Maxwell's equations are solved in Fourier space, i.e. in a basis of plane waves for both polarizations.

We divided the OPV devices into slices in the z-direction, wherein the dielectric function depends periodically on x and y. We obtained the SM for each layer by integrating the Maxwell's equations with continuity boundary conditions. The SM of each layer was convoluted to obtain the SM of the entire structure. The SM yields the total reflectance R (including diffraction), transmittance T (~0) and absorbance A (= 1 – R – T) at each wavelength. This SM technique has advantages over real-space methods in being able to simulate fully 3D geometries, without added memory requirements, since a real space grid is unnecessary. The SM method is fully parallelized with each frequency being sent to a different processor. Experimental values for the wavelength dependent dielectric functions for the materials were utilized.

4.4 Results and Discussion

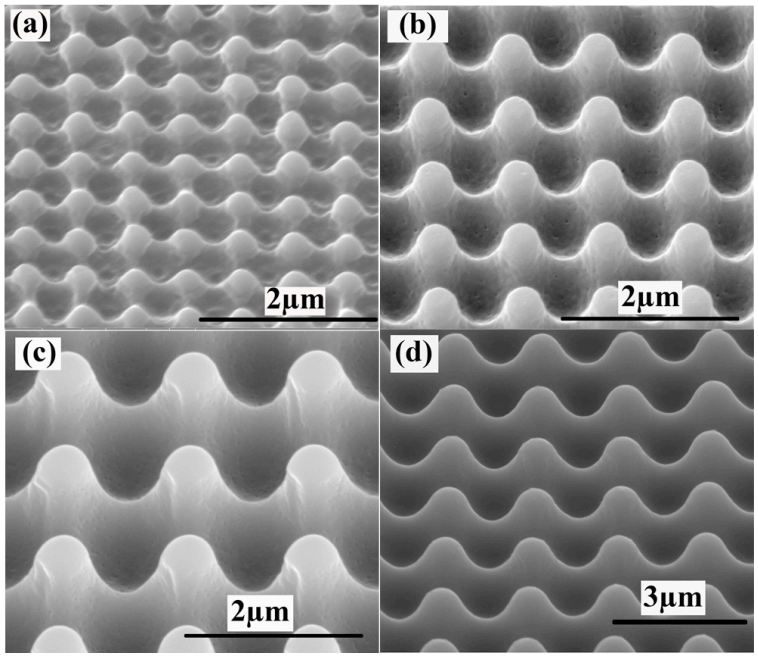

Fig. 35 SEM images of MLAs with pitch sizes (a) 0.6µm, (b) 1µm, (c) 1.5µm, and (d) 2µm.

MLAs with four pitch sizes (0.6 µm, 1 µm, 1.5 µm, and 2 µm with SEM images shown in **Fig. 35** and device structures shown in **Fig. 36**.) were fabricated and evaluated. In order to compare the optical properties of the substrates with and without MLA, the global transmission spectra of these substrates (structure: MLA/glass/ITO) were measured as well as simulated; they are plotted in **Fig. 37**. As the experimental plots in **Fig. 37a** show, all substrates have similar spectra; only the 0.6 µm MLA substrate showed slightly lower transmission between 400 nm and 550 nm wavelengths. This lower transmission is due to stronger scattering of light passing through the 0.6 µm pitch microlenses. We visually observed that part of the scattered light escaped out through the side of the substrates before

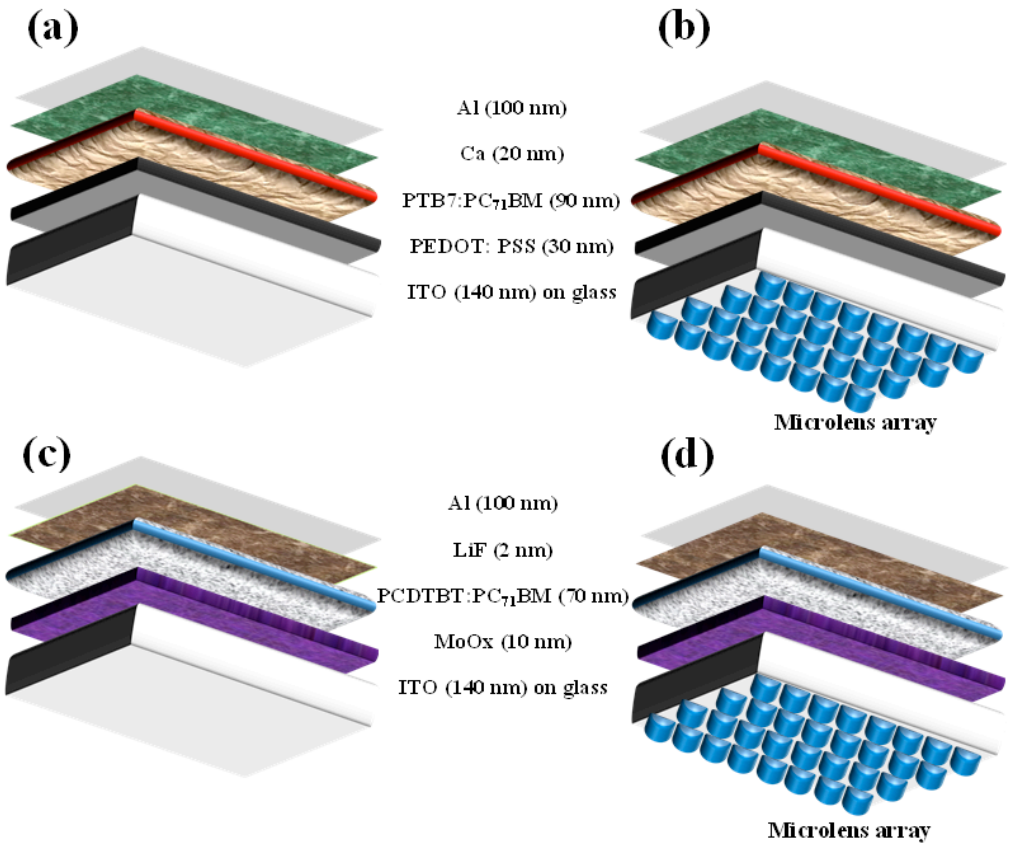

Fig. 36 Schematic diagrams of different devices: (a) PTB7 reference device, (b) PTB7 MLA device, (c) PCDTBT reference device, (d) PCDTBT MLA device.

entering the integrating sphere. Similar amount of light was transmitted through different substrates toward the active-layers. The calculated spectra from simulation support this conclusion. The calculated spectra in **Fig. 37b** are very similar to the experimental data. All substrates have similar global transmission spectra including 0.6 μm MLA substrate, since calculations include the scattered light that escaped in the experiment. The positions of maxima are near 530 nm from multiple interference effects, depending on ITO thickness. Even though all these substrates had similar global transmission spectra, they exhibited very different diffraction patterns. These patterns are shown in the photographs of **Fig. 38**. To obtain these images, devices were illuminated with a white light beam normal to the substrates, through a hole at the bottom. A sheet of white paper was placed next to the devices to project the diffraction patterns. No diffraction pattern was observed for the reference device. The MLA substrates, however, being two-dimensional diffraction gratings, showed rainbow like diffraction patterns. According to the grating equation $dsin\theta_m = m\lambda$,

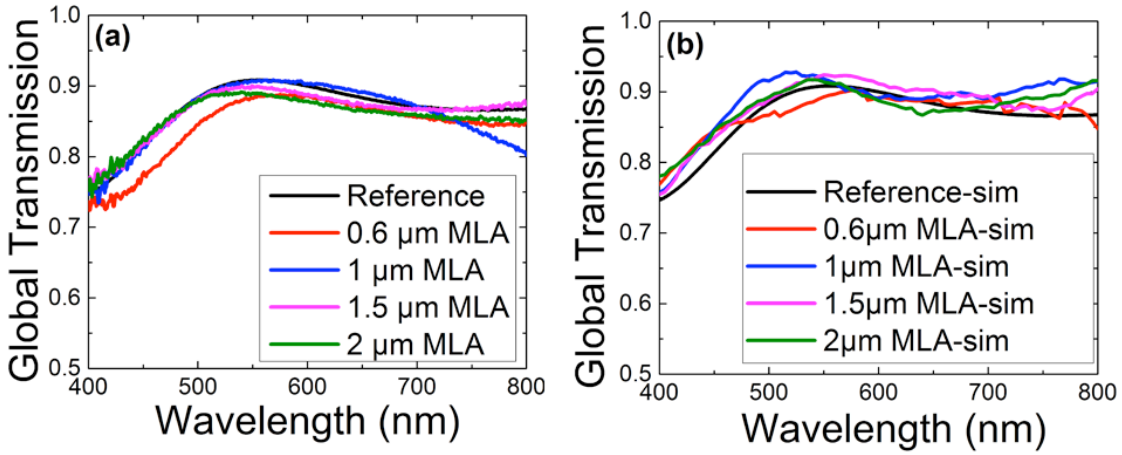

Fig. 37 (a) Experimental and (b) simulated global transmission spectra of substrates without MLA (Reference) and with MLA (0.6 μm, 1 μm, 1.5 μm and 2 μm pitches).

diffraction order m is directly proportional to grating period d. Thus, larger period (pitch) leads to additional diffraction modes. On the other hand, diffraction angle θ_m is inversely proportional to the pitch. Thus, larger pitch leads to decreased spacing between different diffraction orders. Both, additional modes and decreased angles for higher pitches are evident in the photographs of **Fig. 38**.

To characterize the effect of MLAs on the performance of OPV devices, PTB7:$PC_{71}BM$ devices were fabricated on the reference substrate (no MLA) and substrates with MLA of different pitch sizes. Current versus voltage measurements were performed under illumination; the results are plotted in **Fig. 39a**. Open circuit voltages of MLA devices were similar to the reference. However, short circuit current densities (J_{sc}) of all MLA devices were notably higher than the reference. As tabulated in table 1, J_{sc} and PCE of the

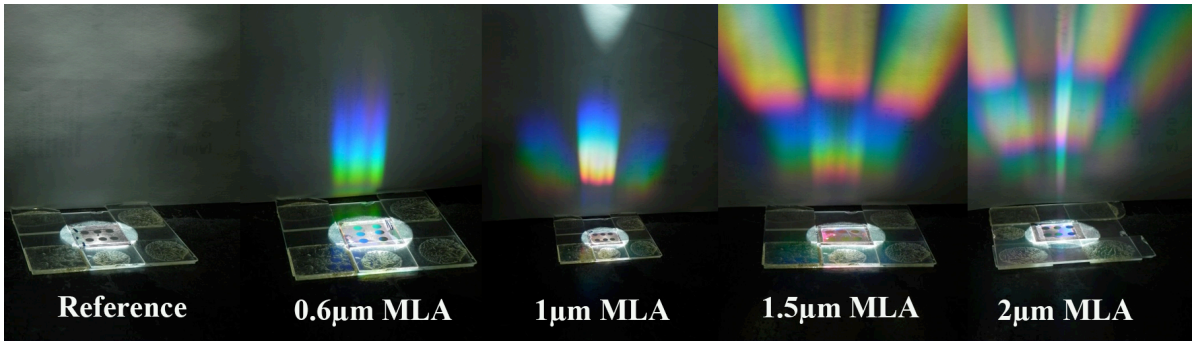

Fig. 38 Photographs of light diffraction patterns through reference and MLA devices.

reference were 16.1 mA/cm2 and 7.73%, respectively, among the highest in literature for PTB7 based devices. Among the MLA devices, devices with 1 µm pitch MLA showed the highest J_{sc} and PCE, 18 mA/cm2 and 8.55%, respectively. J_{sc} and PCE increased going from

Table 2 J_{sc} and PCE of PTB7:$PC_{71}BM$ OPV devices for MLAs of different pitch sizes.

Parameters	Reference	0.6 µm (H=250nm)	1 µm (H=350nm)	1.5 µm (H=900nm)	2 µm (H=1000nm)
J_{sc} (mA/cm^2)	16.10	17.39	18.00	17.70	17.50
J_{sc} enhancement (%)		8.01	11.80	9.94	8.70
PCE (%)	7.73	8.14	8.55	8.25	8.25
PCE enhancement (%)		5.30	10.60	6.73	6.73

0.6 µm pitch MLA to 1 µm pitch MLA, and then slightly decreased for 1.5 µm and 2 µm pitch MLA. The values of heights of all MLAs are also listed in **Table 2**. EQE spectra of the

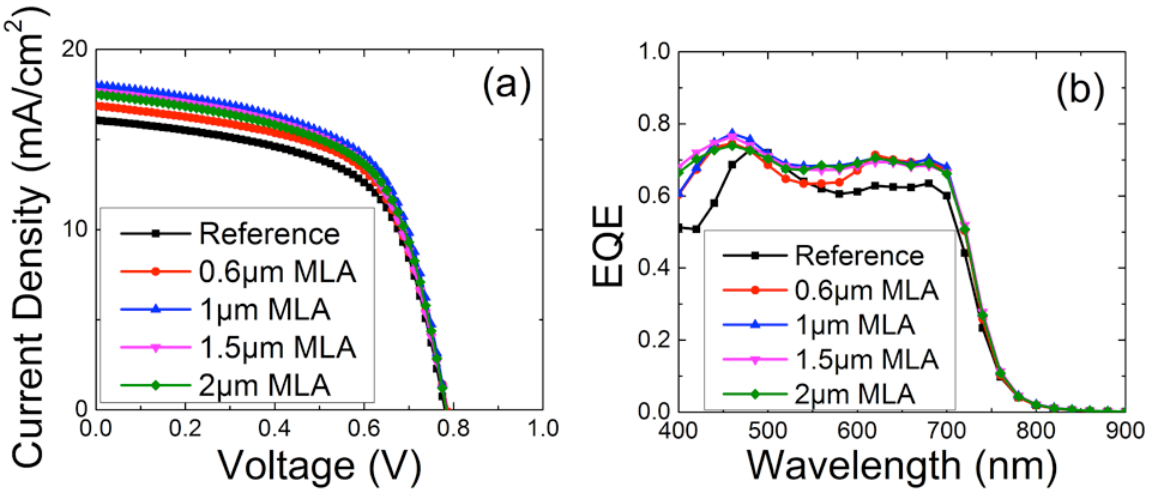

Fig. 39 (a) *JV* curves, and (b) EQE spectra of PTB7 reference and MLA devices (p = 0.6 µm, h = 250 nm; p = 1 µm, h = 350 nm; p = 1.5 µm, h = 900 nm; p = 2 µm, h = 1000 nm).

reference and MLA devices are plotted in **Fig. 39b**. As can be seen, MLA devices exhibit broadband enhancement across the range of wavelengths absorbed by the PTB7:$PC_{71}BM$ system, especially in the 400 - 500 nm and 600 - 800 nm wavelength regions.

In addition to the pitch sizes, heights of microlenses also affected the OPV device performance (**Fig. 40**). To investigate the effect of heights, two to four height values were evaluated experimentally for each pitch. Optical simulations for these dimensions were also performed on corresponding device structures. Different heights for each pitch were realized by intuitive variation of photoresist spin-coating parameters during MLA fabrication; all the heights for a given pitch were such that the height/pitch ratio (h/p ratio) was ≤ 1. **Fig. 40** shows the combined (experimental and simulated) J_{sc} enhancement data for different pitches and heights; enhancement versus height to pitch ratio (h/p ratio) are also plotted. As can be seen, for a given pitch, mostly enhancement increased as the height of MLAs increased.

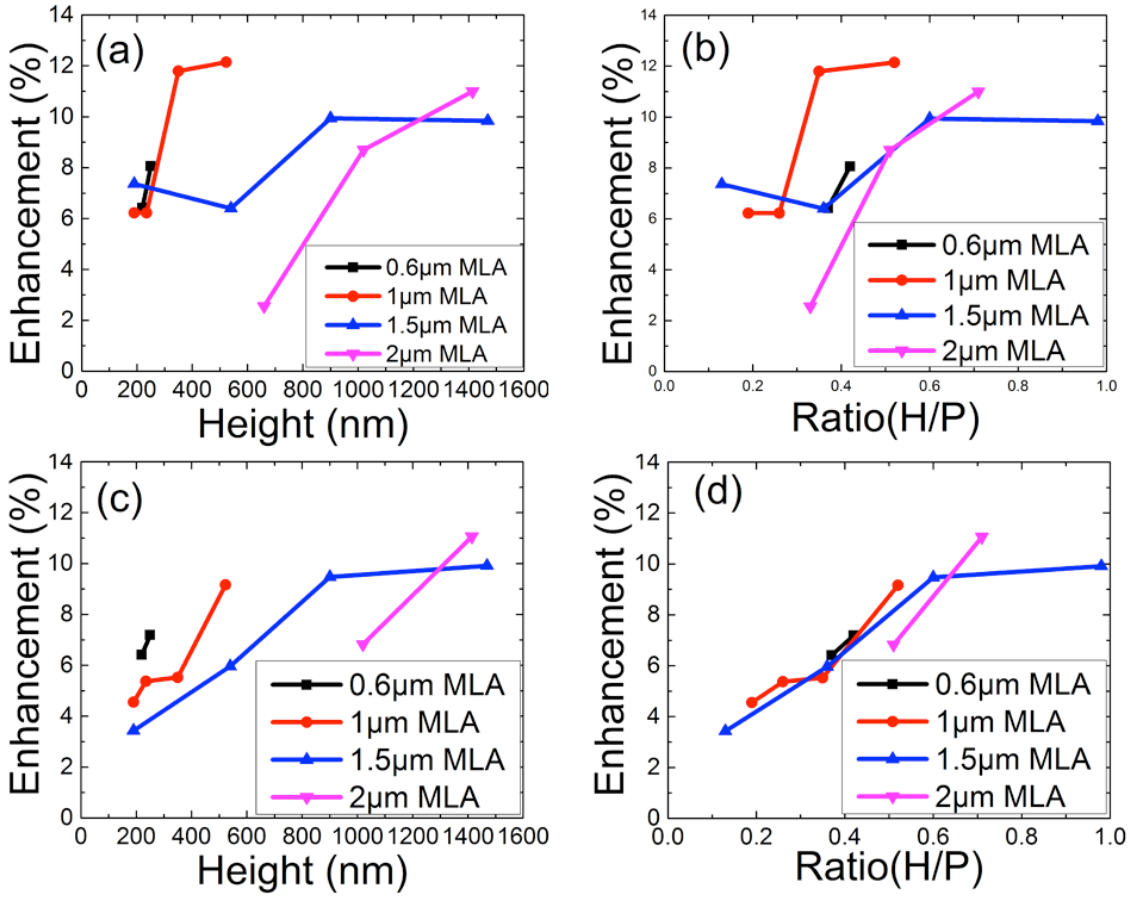

Fig. 40 Enhancement of J_{sc} of PTB7:$PC_{71}BM$ devices for MLA of different pitch sizes as a function of height and height-pitch ratio of MLA: (a, b) experimental results; (c, d) simulation results.

First, we discuss the experimental results of height variations (**Fig. 40a** and **b**). For the 0.6 μm pitch MLA device, J_{sc} enhancement was 6-8% around h/p ratio of 0.4. For the 1 μm pitch MLA device, there was a significant jump in enhancement from 6% to 12% when the h/p ratio increased from 0.2 to 0.4, following which the enhancement began to saturate. The enhancement values increased less sharply with height in the 1.5 μm pitch MLA device; enhancement was ~7% for smaller h/p ratios (0.2 - 0.4), and ~10% for higher h/p ratios (0.6 – 1). In the devices with the largest MLA pitch of 2 μm, the enhancement increased rapidly with increasing h/p ratio, similar to the 1 μm pitch MLA devices. Around the h/p ratio of 0.3,

the enhancement was 2.5%, while it increased to 9% at the ratio of 0.5, and to the highest value of 11% at the ratio of 0.7.

Simulations agree with the experiments on a general trend that for a given MLA pitch, enhancement increases as height increases (**Fig. 40c** and **d**). On the absolute enhancement values, there are some differences between experiments and simulations, which can be due to differences in the MLA structure employed in simulations and the one actually realized by fabrication. Fabricated structures have some unintentional imperfections and local irregularities, examples of which are some depressions in the valleys, as can be seen in SEM images (**Fig. 35**). Nevertheless, simulations agree with measurements on the central trend that enhancement increases with increasing h/p ratio. Simulations also reveal an interesting feature relevant for MLA architecture design: that across different MLA pitches, enhancement values are similar or close for a given h/p ratio. The h/p ratio around 0.4 is a pronounced example of this.

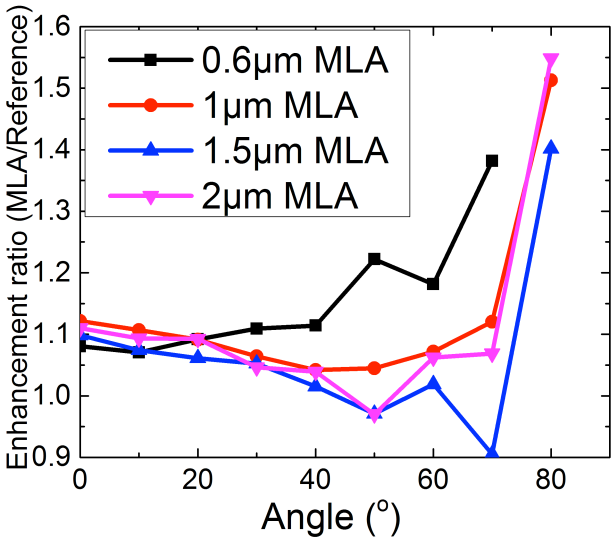

Fig. 41 The J_{sc} enhancement ratio of MLA devices to reference vs. incident light angle.

The current-voltage measurements under illumination are typically done with incident light normal to the substrates. However, for non-tracking PV systems, incident angle of sunlight changes throughout the day. In order to probe the angle dependence, we carried out current-voltage measurements with different incident light angles. Devices were rotated from the normal angle (0^o) to almost parallel to the light source beam (80^o), and J_{sc} was measured at 10^o intervals. Angle dependent enhancement ratios were obtained by dividing J_{sc} of MLA devices by that of the reference device (**Fig. 41**). For the MLA devices with 1 μm, 1.5 μm and 2 μm pitch, enhancement slightly decreases with increasing angle up to 50^o. This is because with increasing angle, light path in the reference device increases. At higher angles though, reflection becomes high for the reference and increasingly less light is absorbed in the active-layer. In contrast, MLA reduces the reflection and enhancement ratios in MLA devices rapidly rise to 1.4 - 1.5 at 80^o. The enhancement ratio for 0.6 μm pitch MLA device

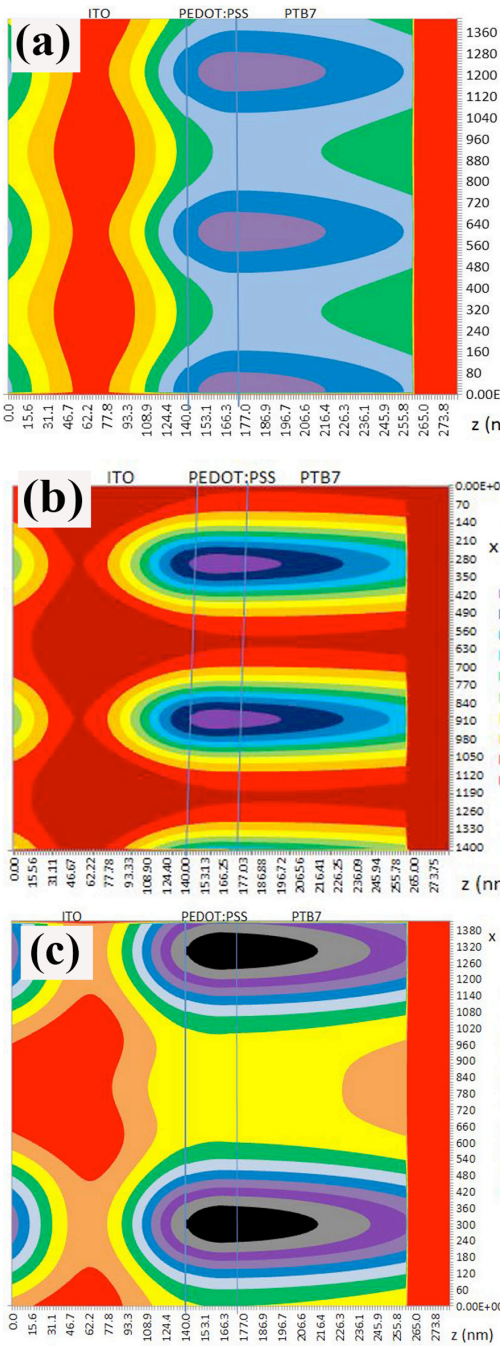

Fig. 42 Simulated electrical field distribution (for wavelength 610 nm) inside the MLA devices with (a) p = 0.6 μm, h = 600 nm, (b) p = 0.6 μm, h = 1000 nm, (c) p = 1 μm, h = 1000 nm.

showed a consistently increasing trend as incident light angle increased, different from devices of other pitch sizes. This might be due to diffraction effects being strongest in the 0.6 μm device. The angle dependence trends had no evident correlation with heights as the h/p ratios of MLA devices were 0.4, 0.5, 1 and 0.7 (for 0.6, 1, 1.5 and 2 μm pitch MLAs, respectively).

To better understand the enhancement mechanisms in MLA devices, electrical field distributions in MLA devices were simulated for different MLA dimensions. Fig. 8 shows the electrical field distribution for 610 nm wavelength in the 0.6 μm and 1 μm pitch MLA devices. To probe the height dependence, two heights were simulated for the 0.6 μm pitch MLA device. One can see that field intensities in the PTB7:$PC_{71}BM$ active layers exhibit a periodic distribution of high intensity focused regions. The incident electrical field intensity was 1. In the 0.6 μm pitch MLA devices (**Fig. 42a** and **b**), as the MLA height increases from 600 nm to 1000 nm, the light focusing increases, which contributes to higher electrical field intensity in the higher height device. However, as the field intensities at the periodic focused spots gets higher, the field intensities in the intermediate regions decrease, even below 1 in some regions. However, overall there is a gain. Comparing **Fig. 42b** and **c**, the MLA height in these two devices is the same at 1000 nm, but (b) has a smaller pitch of 0.6 μm than (c) of 1μm. The maximum field intensity of (b) is slightly larger than that of (c), which agrees with the observed phenomena. Although the focusing regions are closer for the 0.6 μm pitch, portions of the enhanced $|E|^2$ lie in the PEDOT:PSS layer. Thus, there is a trade-off between the spatial separation of the focusing spots dictated by the pitch and the location of the focus spots within the active layer. The balance of this trade-off determines the optimal MLA configuration.

Since the MLA architecture reduces optical losses, we hypothesized that it will be more beneficial for devices with thinner active-layers. In OPV devices based on several contemporary polymers, optimal thicknesses of active-layer are smaller as optimized for charge transport; for example, 60~70 nm thickness in devices based on PCDTBT. To test our hypothesis, we also fabricated MLA and reference devices with PCDTBT polymer. Current-voltage and EQE curves of these devices are plotted in **Fig. 43** and performance parameters

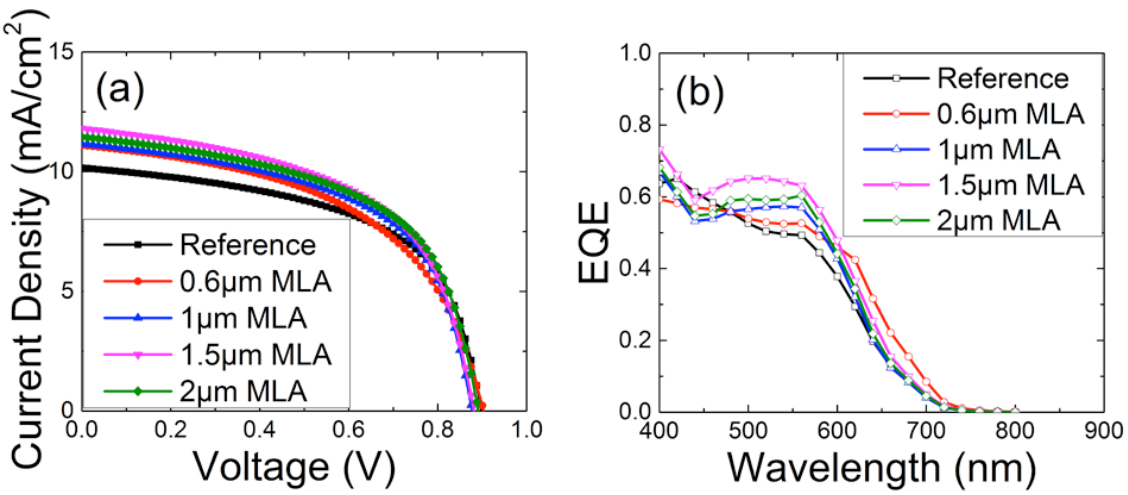

Fig. 43 (a) *JV* curves and (b) EQE spectra of PCDTBT based reference and MLA devices.

are listed in **Table 3**. MLA devices showed very similar open circuit voltage to the reference. However, the J_{sc} of all MLA devices was higher than the reference. As shown in **Table 3**, the reference has J_{sc} of 10.03 mA/cm^2, and PCE of 5.19%. MLA devices showed improvement in J_{sc} by between 10.47% for 0.6 μm MLA to 10.67% for 1 μm pitch MLA. As MLA pitch increased to 1.5 μm, the enhancement increased to 16.95% and then dropped to 13.86% for 2 μm pitch MLA. The enhancement of PCE in MLA devices also increased from 5.59% for 0.6 μm pitch to 7.71% for 1 μm pitch, and then peaks to 13.10% for 1.5 μm and drops to 11.56% for 2 μm MLA. EQE data shows that the MLAs (1μm, 1.5 μm and 2μm) mainly have

Table 3 J_{sc} and PCE of PCDTBT:$PC_{71}BM$ OPV devices for MLAs of different pitch sizes.

Parameters	Reference	0.6 μm (H=250nm)	1 μm (H=350nm)	1.5 μm (H=900nm)	2 μm (H=1000nm)
J_{sc} (mA/cm^2)	10.03	11.08	11.10	11.73	11.42
J_{sc} enhancement (%)		10.47	10.67	16.95	13.86
PCE (%)	5.19	5.48	5.59	5.87	5.79
PCE enhancement (%)		5.59	7.71	13.10	11.56

enhancement in wavelength region of 480 nm – 800 nm. However, there is a drop wavelength between 400 nm and 460 nm. The enhancement from the 0.6 μm MLA is higher in the longer wavelength region of 600 nm – 800 nm than the other MLAs. Comparing the results of PCDTBT with PTB7 devices, one can see that device performance is enhanced more when the active-layer thicknesses are small.

4.5 Conclusion

We demonstrate that by adding a MLA layer on the light-facing side of the transparent substrate in OPV devices, optical absorption in the active-layers improve due to reduced reflection, and increased light path achieved by light focusing and diffraction. Optical field intensity increases at periodical spots inside the active layer. All of these effects combine to enhance short-circuit currents and power conversion efficiencies. We get around 10% enhancements in PTB7:$PC_{71}BM$ devices with MLA pitch size of 0.6 μm, 1 μm, 1.5 μm and 2 μm, even when the reference devices were high efficiency devices with optimized processing conditions. The enhancement generally increases with increasing height of microlenses. When the angle of light incidence changes away from the normal, the enhancements for 1 μm, 1.5 μm or 2 μm pitch MLAs drop slightly, and then increase significantly at large angles. For 0.6 μm pitch MLA, enhancement increases at all non-normal angles. Simulations using the scattering matrix approach support the central

experimental observations and provide insights into the enhancement mechanisms. The enhancement was as high as 17% in PCDTBT based MLA devices. The simple stamping technique to fabricate the MLAs can be scaled readily to larger areas. Moreover, the MLA is on the substrate side opposite to the active layer and does not hinder the cell fabrication or electrical characteristics. It is also generally applicable to all types of solar cells due to its non-intrusive and external nature.

CHAPTER 5.

SUMMARY

In this dissertation, the background of photovoltaic devices and organic photovoltaic devices are introduced. The basic working mechanism, common device structures, polymer materials, and different losses are briefly discussed. Further, chapter 2 elaborates the thickness limitation of organic photovoltaic devices and the importance of having optical methods to trap light in order to reduce optic loss. Followed by this is a very detailed list of the literature works of light trapping methods on OPV. The list incudes antireflection coating, light concentration, photon recycling, novel geometries, front surface coupler, textured substrate, structure back reflector and plasmonic methods. Most of the structure diagrams are included also with the results of light trapping methods.

In chapter 3 and chapter 4, an optical structure - microlens array - was employed to increase light absorption inside the active layer, and PCE of OPV devices increased even for optimized devices. Normal incident light rays are refracted at the MLA and travel longer optical paths inside the active layers. Three OPV systems P3HT:PCBM, PCDTBT:$PC_{71}BM$ and PTB7:$PC_{71}BM$ were investigated. In the P3HT:PCBM system, MLA increased the absorption, absolute external quantum efficiency , and the PCE of an optimized device by ~ 4.3%. In the PCDTBT:$PC_{71}BM$ system, MLA increased the absorption, absolute external quantum efficiency, and PCE by more than 10%. After optimizing the dimension of MLA, we observed up to 17% enhancement in the short circuit current of PCDTBT:$PC_{71}BM$ cells, and 10% enhancement in the short circuit current of PTB7:$PC_{71}BM$ cells. By adding a MLA layer on the light-facing side of the transparent substrate in OPV devices, optical absorption in the active-layers improve due to reduced reflection, and increased light path achieved by

light focusing and diffraction. Optical field intensity increases at periodical spots inside the active layer. All of these effects combine to enhance short-circuit currents and power conversion efficiencies. The effect of microlens dimension on the performance enhancement of PTB7 OPV system was studied. The enhancement generally increases with increasing height-pitch ratio of microlenses. When the angle of light incidence changes away from the normal, the enhancements for 1 μm, 1.5 μm or 2 μm pitch MLAs drop slightly, and then increase significantly at large angles. For 0.6 μm pitch MLA, enhancement increases at all non-normal angles. Simulations using the scattering matrix approach support the central experimental observations and provide insights into the enhancement mechanisms. The simple stamping technique to fabricate the MLAs can be scaled readily to larger areas. Moreover, the MLA is on the substrate side opposite to the active layer and does not hinder the cell fabrication or electrical characteristics. It is also generally applicable to all types of solar cells due to its non-intrusive and external nature.

CHAPTER 6.

REFERENCES

1. H. Roana Melina de Oliveira, L. Yinghui, M. Morten and R. Horst-Günter, *Nanotechnology*, 2013, **24**, 145301.

2. H. A. Atwater and A. Polman, *Nat Mater*, 2010, **9**, 205-213.

3. K. M. Coakley and M. D. McGehee, *Chemistry of Materials*, 2004, **16**, 4533-4542.

4. K. Tvingstedt, S. Dal Zilio, O. Inganäs and M. Tormen, *Opt. Express*, 2008, **16**, 21608-21615.

5. T. D. Heidel, J. K. Mapel, M. Singh, K. Celebi and M. A. Baldo, *Appl Phys Lett*, 2007, **91**, 093506.

6. K. Tvingstedt, V. Andersson, F. Zhang and O. Inganäs, *Appl Phys Lett*, 2007, **91**, 123514.

7. H.-L. Yip and A. K. Y. Jen, *Energ Environ Sci*, 2012, **5**, 5994-6011.

8. M. Niggemann, M. Glatthaar, P. Lewer, C. Müller, J. Wagner and A. Gombert, *Thin Solid Films*, 2006, **511–512**, 628-633.

9. K. Tvingstedt, Z. Tang and O. Inganäs, *Appl Phys Lett*, 2012, **101**, 163902.

10. H. Zhen, K. Li, Z. Huang, Z. Tang, R. Wu, G. Li, X. Liu and F. Zhang, *Appl Phys Lett*, 2012, **100**, 213901.

11. A. J. Morfa, K. L. Rowlen, T. H. Reilly, M. J. Romero and J. van de Lagemaat, *Appl Phys Lett*, 2008, **92**, 013504.

12. K. S. Nalwa, J.-M. Park, K.-M. Ho and S. Chaudhary, *Adv Mater*, 2011, **23**, 112-116.

13. W. Cao, J. D. Myers, Y. Zheng, W. T. Hammond, E. Wrzesniewski and J. Xue, *Appl Phys Lett*, 2011, **99**, 023306.

14. L. Song and A. Uddin, *Optics Express*, 2012, **20**, A606-A621.

15. Z. Hu, J. Zhang and Y. Zhao, *J Appl Phys*, 2012, **111**, 104516.

16. K. Tvingstedt, N.-K. Persson, O. Inganas, A. Rahachou and I. V. Zozoulenko, *Appl Phys Lett*, 2007, **91**, 113514.

17. S. Esiner, T. Bus, M. M. Wienk, K. Hermans and R. A. J. Janssen, *Adv Energy Mater*, 2013, **3**, 1013-1017.

18. D. H. Wang, D.-G. Choi, K.-J. Lee, J.-H. Jeong, S. H. Jeon, O. O. Park and J. H. Park, *Org Electron*, 2010, **11**, 285-290.

19. M. Niggemann, M. Glatthaar, A. Gombert, A. Hinsch and V. Wittwer, *Thin Solid Films*, 2004, **451–452**, 619-623.

20. J. H. Lee, D. W. Kim, H. Jang, J. K. Choi, J. Geng, J. W. Jung, S. C. Yoon and H.-T. Jung, *Small*, 2009, **5**, 2139-2143.

21. L. Müller-Meskamp, Y. H. Kim, T. Roch, S. Hofmann, R. Scholz, S. Eckardt, K. Leo and A. F. Lasagni, *Adv Mater*, 2012, **24**, 906-910.

22. C. Cho, H. Kim, S. Jeong, S.-W. Baek, J.-W. Seo, D. Han, K. Kim, Y. Park, S. Yoo and J.-Y. Lee, *Solar Energy Materials and Solar Cells*, 2013, **115**, 36-41.

23. G. Li, V. Shrotriya, Y. Yao and Y. Yang, *J Appl Phys*, 2005, **98**.

24. M. K. Siddiki, J. Li, D. Galipeau and Q. Q. Qiao, *Energ Environ Sci*, 2010, **3**, 867-883.

25. G. Li, V. Shrotriya, J. S. Huang, Y. Yao, T. Moriarty, K. Emery and Y. Yang, *Nature Materials*, 2005, **4**, 864-868.

26. J. M. Roney, Earth Policy Institute, Washington, 2014.

27. J. Perlin, *From Space to Earth: The Story of Solar Electricity*, Harvard University Press, 1999.

28. H. Akamatu, H. Inokuchi and Y. Matsunaga, *Nature*, 1954, **173**, 168-169.

29. M. P. a. C. E. Swenberg, *Electronic Processes in Organic Crystals and Polymers*, Oxford University Press, New York, 1999.

30. H. Shirakawa, E. J. Louis, A. G. MacDiarmid, C. K. Chiang and A. J. Heeger, *Journal of the Chemical Society, Chemical Communications*, 1977, 578-580.

31. M. Pope and C. E. Swenberg, *Electronic Processes in Organic Crystals and Polymers*, Oxford University Press, 1999.

32. NREL, Best Research Cell Efficiency Records, http://www.nrel.gov/ncpv/images/efficiency_chart.jpg, Decemeber 3, 2014.

33. Z. He, C. Zhong, S. Su, M. Xu, H. Wu and Y. Cao, *Nat Photon*, 2012, **6**, 593-597.

34. D. Gendron and M. Leclerc, *Energ Environ Sci*, 2011, **4**, 1225-1237.

35. S. Günes, H. Neugebauer and N. S. Sariciftci, *Chemical reviews*, 2007, **107**, 1324-1338.

36. R. Kroon, M. Lenes, J. C. Hummelen, P. W. M. Blom and B. de Boer, *Polymer Reviews*, 2008, **48**, 531-582.

37. E. L. Ratcliff, B. Zacher and N. R. Armstrong, *J Phys Chem Lett*, 2011, **2**, 1337-1350.

38. R. Po, C. Carbonera, A. Bernardi and N. Camaioni, *Energ Environ Sci*, 2011, **4**, 285-310.

39. J. A. Carr, Y. Chen, M. Elshobaki, R. C. Mahadevapuram and S. Chaudhary, *Nanomaterials and Energy*, 2011, **1**, 18-26.

40. J. Jo, S.-S. Kim, S.-I. Na, B.-K. Yu and D.-Y. Kim, *Advanced Functional Materials*, 2009, **19**, 866-874.

41. M. Campoy-Quiles, T. Ferenczi, T. Agostinelli, P. G. Etchegoin, Y. Kim, T. D. Anthopoulos, P. N. Stavrinou, D. D. C. Bradley and J. Nelson, *Nat Mater*, 2008, **7**, 158-164.

42. G. Li, V. Shrotriya, Y. Yao, J. Huang and Y. Yang, *J Mater Chem*, 2007, **17**, 3126-3140.

43. H. Hoppe and N. S. Sariciftci, *J Mater Chem*, 2006, **16**, 45-61.

44. L. Goris, A. Poruba, L. Hod'akova, M. Vanecek, K. Haenen, M. Nesladek, P. Wagner, D. Vanderzande, L. De Schepper and J. V. Manca, *Appl Phys Lett*, 2006, **88**, 052113-052113.

45. P. W. M. Blom, V. D. Mihailetchi, L. J. A. Koster and D. E. Markov, *Adv Mater*, 2007, **19**, 1551-1566.

46. H. Hoppe, S. Shokhovets and G. Gobsch, *physica status solidi (RRL) – Rapid Research Letters*, 2007, **1**, R40-R42.

47. G. F. A. Dibb, M.-A. Muth, T. Kirchartz, S. Engmann, H. Hoppe, G. Gobsch, M. Thelakkat, N. Blouin, S. Tierney, M. Carrasco-Orozco, J. R. Durrant and J. Nelson, *Sci. Rep.*, 2013, **3**.

48. J. Peet, L. Wen, P. Byrne, S. Rodman, K. Forberich, Y. Shao, N. Drolet, R. Gaudiana, G. Dennler and D. Waller, *Appl Phys Lett*, 2011, **98**, 043301.

49. R. A. Street and M. Schoendorf, *Physical Review B*, 2010, **81**, 205307.

50. R. S. Crandall, *J Appl Phys*, 1982, **53**, 3350-3352.

51. M. Lenes, L. J. A. Koster, V. D. Mihailetchi and P. W. M. Blom, *Appl Phys Lett*, 2006, **88**, 243502-243503.

52. R. A. Street, A. Krakaris and S. R. Cowan, *Advanced Functional Materials*, 2012, **22**, 4608-4619.

53. G. Dennler, M. C. Scharber and C. J. Brabec, *Adv Mater*, 2009, **21**, 1323-1338.

54. D. Credgington, R. Hamilton, P. Atienzar, J. Nelson and J. R. Durrant, *Advanced Functional Materials*, 2011, **21**, 2744-2753.

55. S. Lee, S. Nam, H. Kim and Y. Kim, *Appl Phys Lett*, 2010, **97**, 103503.

56. S. C. Price, A. C. Stuart, L. Yang, H. Zhou and W. You, *Journal of the American Chemical Society*, 2011, **133**, 4625-4631.

57. H. Hoppe, N. Arnold, N. S. Sariciftci and D. Meissner, *Solar Energy Materials and Solar Cells*, 2003, **80**, 105-113.

58. B. V. Andersson, D. M. Huang, A. J. Moulé and O. Inganäs, *Appl Phys Lett*, 2009, **94**, 043302.

59. J. D. Kotlarski, P. W. M. Blom, L. J. A. Koster, M. Lenes and L. H. Slooff, *J Appl Phys*, 2008, **103**, 084502.

60. M. Soldera, K. Taretto and T. Kirchartz, *physica status solidi (a)*, 2012, **209**, 207-215.

61. S. E. Shaheen, C. J. Brabec, N. S. Sariciftci, F. Padinger, T. Fromherz and J. C. Hummelen, *Appl Phys Lett*, 2001, **78**, 841-843.

62. G. Li, R. Zhu and Y. Yang, *Nat Photon*, 2012, **6**, 153-161.

63. J. Nelson, *The Physics of Solar Cells*, Imperial College Press, 2003.

64. K. Forberich, G. Dennler, M. C. Scharber, K. Hingerl, T. Fromherz and C. J. Brabec, *Thin Solid Films*, 2008, **516**, 7167-7170.

65. W. Zhou, M. Tao, L. Chen and H. Yang, *J Appl Phys*, 2007, **102**, 103105.

66. D. Bouhafs, A. Moussi, A. Chikouche and J. M. Ruiz, *Solar Energy Materials and Solar Cells*, 1998, **52**, 79-93.

67. W. H. Southwell, *Opt. Lett.*, 1983, **8**, 584-586.

68. P. Campbell and M. A. Green, *J Appl Phys*, 1987, **62**, 243-249.

69. J. Zhao and M. A. Green, *Electron Devices, IEEE Transactions on*, 1991, **38**, 1925-1934.

70. J. Zhao, A. Wang, P. Campbell and M. A. Green, *Electron Devices, IEEE Transactions on*, 1999, **46**, 1495-1497.

71. J. Kalowekamo and E. Baker, *Solar Energy*, 2009, **83**, 1224-1231.

72. R. Koeppe, N. S. Sariciftci and A. Buchtemann, *Appl Phys Lett*, 2007, **90**, 181126-181126-181123.

73. M. Niggemann, M. Riede, A. Gombert and K. Leo, *physica status solidi (a)*, 2008, **205**, 2862-2874.

74. V. Andersson, K. Tvingstedt and O. Inganäs, *J Appl Phys*, 2008, **103**, 094520.

75. B. V. Andersson, U. Wuerfel and O. Inganäs, *Solar Energy*, 2011, **85**, 1257-1263.

76. S. J. Kim, G. Y. Margulis, S.-B. Rim, M. L. Brongersma, M. D. McGehee and P. Peumans, *Optics Express*, 2013, **21**, A305-A312.

77. S.-B. Rim, S. Zhao, S. R. Scully, M. D. McGehee and P. Peumans, *Appl Phys Lett*, 2007, **91**, 243501-243503.

78. Y. Zhou, F. Zhang, K. Tvingstedt, W. Tian and O. Inganäs, *Appl Phys Lett*, 2008, **93**, 033302.

79. C. Eisele, C. E. Nebel and M. Stutzmann, *J Appl Phys*, 2001, **89**, 7722-7726.

80. F. Llopis and I. Tobías, *Solar Energy Materials and Solar Cells*, 2005, **87**, 481-492.

81. H. L. Chen, K. T. Huang, C. H. Lin, W. Y. Wang and W. Fan, *Microelectronic Engineering*, 2007, **84**, 750-754.

82. C. Elsner, J. Zajadacz and K. Zimmer, *Microelectronic Engineering*, 2011, **88**, 60-63.

83. S. Gilles, M. Meier, M. Prömpers, A. v. d. Hart, C. Kügeler, A. Offenhäusser and D. Mayer, *Microelectronic Engineering*, 2009, **86**, 661-664.

84. C. Cocoyer, L. Rocha, L. Sicot, B. Geffroy, R. de Bettignies, C. Sentein, C. Fiorini-Debuisschert and P. Raimond, *Appl Phys Lett*, 2006, **88**, 133108.

85. J. B. Kim, P. Kim, N. C. Pegard, S. J. Oh, C. R. Kagan, J. W. Fleischer, H. A. Stone and Y.-L. Loo, *Nat Photon*, 2012, **6**, 327-332.

86. D.-H. Ko, J. R. Tumbleston, A. Gadisa, M. Aryal, Y. Liu, R. Lopez and E. T. Samulski, *J Mater Chem*, 2011, **21**, 16293-16303.

87. Y. Yang, K. Mielczarek, M. Aryal, A. Zakhidov and W. Hu, *ACS Nano*, 2012, **6**, 2877-2892.

88. Z. Tang, A. Elfwing, J. Bergqvist, W. Tress and O. Inganäs, *Adv Energy Mater*, 2013, **3**, 1606-1613.

89. L. Stolz Roman, O. Inganäs, T. Granlund, T. Nyberg, M. Svensson, M. R. Andersson and J. C. Hummelen, *Adv Mater*, 2000, **12**, 189-195.

90. S.-I. Na, S.-S. Kim, J. Jo, S.-H. Oh, J. Kim and D.-Y. Kim, *Advanced Functional Materials*, 2008, **18**, 3956-3963.

91. S.-I. Na, S.-S. Kim, S.-S. Kwon, J. Jo, J. Kim, T. Lee and D.-Y. Kim, *Appl Phys Lett*, 2007, **91**, 173509.

92. Z. Yu, A. Raman and S. Fan, *Proceedings of the National Academy of Sciences*, 2010, **107**, 17491-17496.

93. D. M. N. M. Dissanayake, A. A. D. T. Adikaari, R. J. Curry, R. A. Hatton and S. R. P. Silva, *Appl Phys Lett*, 2007, **90**, 253502.

94. D. M. N. M. Dissanayake, A. A. D. T. Adikaari and S. R. P. Silva, *Appl Phys Lett*, 2008, **92**, 093308.

95. Z. Rang, A. Haraldsson, D. M. Kim, P. P. Ruden, M. I. Nathan, R. J. Chesterfield and C. D. Frisbie, *Appl Phys Lett*, 2001, **79**, 2731-2733.

96. C. F. Bohren, E. E. Clothiaux and D. R. Huffman, *Absorption and Scattering of Light by Small Particles*, Wiley-VCH, 2010.

97. J. Mertz, *J. Opt. Soc. Am. B*, 2000, **17**, 1906-1913.

98. H. R. Stuart and D. G. Hall, *Appl Phys Lett*, 1996, **69**, 2327-2329.

99. H. R. Stuart and D. G. Hall, *Appl Phys Lett*, 1998, **73**, 3815-3817.

100. D. M. Schaadt, B. Feng and E. T. Yu, *Appl Phys Lett*, 2005, **86**, 063106.

101. D. Derkacs, S. H. Lim, P. Matheu, W. Mar and E. T. Yu, *Appl Phys Lett*, 2006, **89**, 093103.

102. P. Matheu, S. H. Lim, D. Derkacs, C. McPheeters and E. T. Yu, *Appl Phys Lett*, 2008, **93**, 091107.

103. K. Nakayama, K. Tanabe and H. A. Atwater, *Appl Phys Lett*, 2008, **93**, 121904.

104. K. R. Catchpole and A. Polman, *Appl Phys Lett*, 2008, **93**, 191113.

105. K. R. Catchpole and A. Polman, *Optics Express*, 2008, **16**, 21793-21800.

106. F. J. Beck, A. Polman and K. R. Catchpole, *J Appl Phys*, 2009, **105**, 114310.

107. S. H. Lim, W. Mar, P. Matheu, D. Derkacs and E. T. Yu, *J Appl Phys*, 2007, **101**, 104309.

108. S. Mokkapati, F. J. Beck, A. Polman and K. R. Catchpole, *Appl Phys Lett*, 2009, **95**, 053115.

109. K. R. Catchpole and S. Pillai, *J Appl Phys*, 2006, **100**, 044504.

110. B. P. Rand, P. Peumans and S. R. Forrest, *J Appl Phys*, 2004, **96**, 7519-7526.

111. S.-S. Kim, S.-I. Na, J. Jo, D.-Y. Kim and Y.-C. Nah, *Appl Phys Lett*, 2008, **93**, 073307.

112. N. C. Lindquist, W. A. Luhman, S.-H. Oh and R. J. Holmes, *Appl Phys Lett*, 2008, **93**, 123308.

113. V. E. Ferry, L. A. Sweatlock, D. Pacifici and H. A. Atwater, *Nano Lett*, 2008, **8**, 4391-4397.

114. J. K. Mapel, M. Singh, M. A. Baldo and K. Celebi, *Appl Phys Lett*, 2007, **90**, 121102.

115. F.-J. Haug, T. Söderström, O. Cubero, V. Terrazzoni-Daudrix and C. Ballif, *J Appl Phys*, 2008, **104**, 064509.

116. A. Peer and R. Biswas, *ACS Photonics*, 2014, **1**, 840-847.

117. T. Kirchartz, K. Taretto and U. Rau, *The Journal of Physical Chemistry C*, 2009, **113**, 17958-17966.

118. O. V. Mikhnenko, H. Azimi, M. Scharber, M. Morana, P. W. M. Blom and M. A. Loi, *Energ Environ Sci*, 2012, **5**, 6960-6965.

119. D. Duche, P. Torchio, L. Escoubas, F. Monestier, J.-J. Simon, F. Flory and G. Mathian, *Solar Energy Materials and Solar Cells*, 2009, **93**, 1377-1382.

120. H. Shen, P. Bienstman and B. Maes, *J Appl Phys*, 2009, **106**, 073109.

121. J. D. Myers, W. Cao, V. Cassidy, S.-H. Eom, R. Zhou, L. Yang, W. You and J. Xue, *Energ Environ Sci*, 2012, **5**, 6900-6904.

122. J.-M. Park, Z. Gan, W. Y. Leung, R. Liu, Z. Ye, K. Constant, J. Shinar, R. Shinar and K.-M. Ho, *Opt. Express*, 2011, **19**, A786-A792.

123. T.-Y. Chu, S. Alem, P. G. Verly, S. Wakim, J. Lu, Y. Tao, S. Beaupre, M. Leclerc, F. Belanger, D. Desilets, S. Rodman, D. Waller and R. Gaudiana, *Appl Phys Lett*, 2009, **95**, 063304.

124. Z.-Y. Li and L.-L. Lin, *Physical Review E*, 2003, **67**, 046607.

125. Z. Ye, X. Hu, M. Li, K.-M. Ho and P. Yang, *Appl Phys Lett*, 2006, **89**, 241108.

126. ISU, ISU TMM Photonic Software Package, http://www.techtransfer.iastate.edu/en/for_industry/technology_search/search.cfm?fuseaction=technology.details&id=3336, December 3, 2014.

127. C. M. Ramsdale and N. C. Greenham, *Journal of Physics D: Applied Physics*, 2003, **36**, L29.

128. H. Hoppe, N. S. Sariciftci and D. Meissner, *Molecular Crystals and Liquid Crystals*, 2002, **385**, 113-119.

129. Y. Sun, C. J. Takacs, S. R. Cowan, J. H. Seo, X. Gong, A. Roy and A. J. Heeger, *Adv Mater*, 2011, **23**, 2226-2230.

130. R. Gaudiana and C. Brabec, *Nat Photonics*, 2008, **2**, 287-289.

131. R. Biswas and E. Timmons, *Optics Express*, 2013, **21**, A841-A846.

132. Y. Jingbi, L. Xuanhua, X. Feng-xian, E. I. S. Wei, H. W. K. Johnson, L. Gang, C. H. C. Wallace and Y. Yang, *Adv Energy Mater*, 2012, **2**, 1203-1207.

133. S. Vedraine, P. Torchio, D. Duché, F. Flory, J.-J. Simon, J. Le Rouzo and L. Escoubas, *Solar Energy Materials and Solar Cells*, 2011, **95, Supplement 1**, S57-S64.

134. F. Galeotti, W. Mróz, G. Scavia and C. Botta, *Org Electron*, 2013, **14**, 212-218.

135. J. B. Kim, J. H. Lee, C. K. Moon, S. Y. Kim and J. J. Kim, *Adv Mater*, 2013, **25**, 3571-3577.

136. Y. Sun and S. R. Forrest, *J Appl Phys*, 2006, **100**, 073106.

137. E. Wrzesniewski, S.-H. Eom, W. Cao, W. T. Hammond, S. Lee, E. P. Douglas and J. Xue, *Small*, 2012, **8**, 2647-2651.

138. Y. Chen, M. Elshobaki, Z. Ye, J.-M. Park, M. A. Noack, K.-M. Ho and S. Chaudhary, *Phys Chem Chem Phys*, 2013, **15**, 4297-4302.

139. R. Biswas and C. Xu, *Optics Express*, 2011, **19**, A664-A672.